NASA CONTRACTOR REPORT

OBSERVABLES FOR ANTICIPATING TORNADOGENESIS IN MESOCYCLONES

By G. Carrier, F. Fendell, J. Mitchell, and M. Bronstein

Center for Propulsion Technology and Fluid Mechanics
TRW Space & Electronics Group
One Space Park
Redondo Beach, CA 90278

Final Report

November 1992

Prepared for

NASA-George C. Marshall Space Flight Center
Marshall Space Flight Center, Alabama 35812

R5 92.019

NASA

Report Documentation Page

1. Report No.	2. Government Accession No.	3. Recipient's Catalog No.

4. Title and Subtitle
Observables for Anticipating Tornadogenesis in Mesocyclones

5. Report Date
November 1992

6. Performing Organization Code

7. Author(s)
G. Carrier, F. Fendell, J. Mitchell, and M. Bronstein

8. Performing Organization Report No.

10. Work Unit No.

9. Performing Organization Name and Address
TRW Space & Electronics Group
One Space Park
Redondo Beach, CA 90278

11. Contract or Grant No.
NAS8-39049

13. Type of Report and Period Covered
Final Report
July 1991-November 1992

12. Sponsoring Agency Name and Address
National Aeronautics and Space Administration

14. Sponsoring Agency Code

15. Supplementary Notes

16. Abstract
We seek to identify an observable for anticipating tornadogenesis in mesocyclones, because such tornadoes are characterized by particularly long life, long and wide path, and high wind speed. We associate tornadogenesis with the transition from a one-cell vortex to a two-cell vortex. In such a transition, "insertion" of a virtually nonrotating, slowly recirculating core displaces that high-swirl-speed air which is rapidly ascending along a moist-adiabatic locus of thermodynamic states, to an annulus at small but finite distance from the axis of rotation. Such a transition, on vastly larger lateral scale, is known to characterize intensification of a tropical storm to a typhoon. We examine analytically a quasisteady axisymmetric model of a four-part vortex structure consisting of a bulk potential vortex, near-ground inflow layer, "eyewall", and "eye". We inquire whether such a four-part intense vortex, formed in convectively unstably stratified air, is selfsustaining. In particular, we inquire whether the vertical profile of the angular momentum at the periphery is a discriminant for identifying selfsustaining vortices.

17. Key Words (Suggested by Author(s))
Mesocyclones
Severe Local Storms
Supercell Thunderstorms
Tornadogenesis

18. Distribution Statement
Unclassified-Unlimited

19. Security Classif. (of this report)	20. Security Classif. (of this page)	21. No. of pages	22. Price
Unclassified-Unlimited	Unclassified-Unlimited	60	

CONTENTS

LIST OF FIGURES

1. INTRODUCTION

We adopt an idealized model of an intense tall axisymmetric vortex in a stratified "moist atmosphere" above a ground plane, and then analyze the flow to ascertain whether the vortex could be selfsustaining. The ultimate objective is the identification of (hopefully satellite-accessible) observables for anticipating tornadogenesis within a supercell thunderstorm.

In undertaking this work, we note the assessment of Rotunno (1986) that, while aircraft and multi-Doppler radar with a resolution of few kilometers have increased understanding on the 10-50-km thunderstorm scale, the more difficult question of how the larger tornado cyclone produces the smaller-scale tornado is unresolved. "Given the present state of computers, it is impossible for three-dimensional cloud models, even with nested grids, to simulate both the supercell on a domain large enough to include the undisturbed environment and the tornado with a resolution fine enough to capture the significant dynamical processes. However, even if this were possible, the results of such a calculation might be too difficult to handle." (Rotunno 1986, p. 427.)

Supercell-spawned tornadoes have the highest wind speeds, the longest and widest paths, and the longest life-span of any tornadoes, and, thus, from a practical point of view, are the most important (Rotunno 1986). We know that severe weather arises in convectively unstable ambients (i.e., tropospheric stratifications in which the low-level air is particularly warm and moist, so there is a pronounced midtropospheric minimum in the total static enthalpy) (Darkow 1986). However, convective instability only sometimes results in a supercell thunderstorm, and perhaps only one in four supercell thunderstorms spawns a tornado. Thus, a tornado warnings based on mesocyclone detection by dual-Doppler radar would seem likely to incur a significant false-alarm rate, although mesocyclones often manifest some type of severe weather (Brown 1987).

Identifying a further discriminant for tornadogenesis in already well-developed, rotating, severe local storms remains a worthwhile goal. Inquiring into the vertical-vorticity-amplification mechanisms responsible for the pretornadic organization of the rotating thunderstorm seems nonessential for this objective; the organization may be viewed as a given "initial condition".

Rotunno notes that, in the present state of limited understanding of the asymmetric heterogeneous flow in the storm, guidance often is sought from examining the axisymmetric homogeneous flow in a cylindrically configured laboratory apparatus called a vortex chamber (Maxworthy 1982). Fluid within such a chamber is drawn through it by suction applied at an exhaust hole in one end wall, and rotation is added to new fluid, which enters through the lateral surface of the chamber. Clearly, both the primary flow (circulation) and the secondary flow (inflow-updraft-outflow) are very highly constrained in a vortex chamber, and the circulation

added to entering air typically does not vary with height. Thermodynamically, there is no condensation of water vapor, and no density stratification with altitude because of the limited height of the chamber. The laboratory vortex chamber may be of value for investigating specific, purely fluid-dynamical aspects, such as the mass exchange between contiguous "columns" of air (with differential rotation) in a vortex, although artifacts of the apparatus could be misleading about other properties of an intense atmospheric vortex. In our concluding remarks, we suggest a further aspect of tornado dynamics that may be usefully pursued in a laboratory vortex chamber.

For elucidating the thermohydrodynamics of tornadogenesis, we adopt a model of rapidly swirling flow that: extends over the vertical scale of the troposphere; is axisymmetric (for analytic convenience); and involves moist air (with both static temperature and dew-point temperature stratified in accord with atmospheric soundings) which undergoes idealized processes. In selecting appropriate idealized processes, we note that the inferred peak swirl speed, relative to the axis of rotation, in the exceptional, intense tornado (of interest here) may exceed 100 m/s. We believe that the only plausible tropospheric mechanism for attaining the magnitude of lateral pressure deficit (near ground level) consistent with such high swirl speed is the "two-cell", "eye"-within-an-"eyewall" structure known to be associated with hurricane-stage tropical cyclones (Fendell 1974). We suggest that some phenomena associated with the intensification of a tropical storm into a hurricane-stage tropical cyclone also occur during tornadogenesis in a mesocyclone, albeit on vastly reduced lateral scale (Dergarabedian and Fendell 1970, 1971a, 1971b, 1977; Walko 1988). Specifically, we associate tornadogenesis with the (at least partial) insertion of a central column of dry, only very slowly rotating, very slowly recirculating air, characterized by a nearly dry-adiabatic locus of thermodynamic states, within an annulus of mostly saturated, rapidly rotating and ascending air, characterized by a nearly moist-adiabatic locus of thermodynamic states (Figs. 1 and 2). Of course, the idealization of a nearly dry "eye" and an entrainment-free "eyewall" is a convenient simplification that assists both the exposition and the analysis below; relaxation from this idealization may be the subject of subsequent studies. The compatibility of exceptional swirl speeds with this just-described two-cell structure has been previously reported by considering measured, convectively unstable ambients under simplifying cyclostrophic and hydrostatic approximations.

2. OBJECTIVE AND MODEL

Our objective is to examine a further point about the above-described swirling flow by applying the laws of dynamics and thermodynamics. We inquire whether only certain stratifications of the ambient angular momentum at the periphery of the flow permit the two-cell structure, requisite for intense swirl speeds of roughly 100 m/s, to persist. For example, perhaps

a two-cell structure is plausibly sustainable only if the low-level angular momentum at the perimeter persists on a scale equal to the height of the troposphere.

We adopt the model in Fig. 3 for investigating the conjecture of the last paragraph. Although we undertake no transient analysis, we believe that the adopted four-part quasisteady structure might well evolve after spin-up from "reasonable" initial conditions. The top of the flow (say, near 15 km or so) is defined to be an isothermal isobaric horizontal plane, located at an altitude at which the value of the ground-level total static enthalpy is virtually recovered, for the convectively unstable stratification holding at the "lateral edge" (or periphery) of the flow field. At the periphery, the static temperature, the dew-point temperature, and the angular momentum are explicitly given (or are readily deducible) as functions of altitude above the ground plane. (As noted, at the periphery, we typically shall adopt temperature and dew-point-temperature profiles measured in temporal and spatial proximity to a tornadic thunderstorm.) The ground plane is an impervious isothermal plane at which the no-slip boundary condition holds. In the next paragraph, we provide more detail on the quasisteady four-part structure, depicted in Fig. 3; much of the remainder of this investigation then seeks to identify the ambient conditions under which the four-part structure is plausible, stable, and compatible with thermohydrodynamic principles.

Most of the flow (except near the ground plane and the axis of rotation) would consist of warm moist air rotating in a potential vortex in a cyclostrophic, hydrostatic balance, such that isobars would dip groundward as the (cylindrical) radial distance from the axis of symmetry (and rotation) decreases (region I of Fig. 3). There is very little radial motion in the spun-up potential vortex, and only a relatively slow downflux into a nonlinear frictional layer (region II), contiguous to the ground plane. The frictional-layer thickness increases modestly (to, say, 50 m or so) with decreasing radial distance from the axis. Rotating flux that descends into this frictional layer flows radially inward within the layer; in fact, for an intense vortex, at smaller radial distances from the axis of symmetry, frictional effects are significant only in an ever-thinning sublayer immediately contiguous to the ground plane, and most of the inflow-layer thickness can be described by inviscid dynamics. The swirling inflow layer separates at a finite radial distance (say, at radius of 50-75 m) to become a swirling annular updraft of saturated air (the "eyewall", region III). The very-low-altitude corner-like flow of region III is henceforth referred to as the turnaround, and is treated separately below by specializing the relations holding more generally over the vertical extent of the eyewall. In Fig. 3, the eyewall becomes thicker, and tilts away from the axis, with increasing altitude; the updraft may well be sufficiently vigorous that little condensate falls out. Within the updraft annulus is a central column (the "eye", region IV) of warm, dry, slowly recirculating, only very slowly rotating air. For a finite amount of warm moist air available for throughput, the swirling effectively dies (or at least is very diminished) after all the outer-vortex

fluid has been "processed", owing to the frictional loss of angular momentum in the near-ground-level-inflow layer.

3. A MODEL FOR THE ANNULAR ROTATING UPDRAFT

A transversely averaged model for the "eyewall" (region III) is given by the following set of coupled algebraic and differential equations [previously presented in more cumbersome form and without solution (Carrier et al. 1984)]:

conservation of mass (with entrainment from the eye into the eyewall),

$$\rho\, q\, R\, h = \rho_o\, q_o\, R_o\, h_o + \alpha_E \int_0^z \rho_{eye}(z_1)\, q(z_1)\, [R(z_1) - h(z_1)]\, dz_1 \; ; \tag{1}$$

conservation of angular momentum,

$$Rv = R_o\, v_o \; ; \tag{2}$$

conservation of radial momentum across the annulus,

$$\frac{\rho\, q^2\, h}{[1 + (dR/dz)^2]^{3/2}} \frac{d^2R}{dz^2} - \frac{\rho\, v^2\, h}{R[1 + (dR/dz)^2]^{1/2}} + p_{amb} - p_{eye} = 0 \; ; \tag{3}$$

Bernoulli's equation,

$$\frac{q^2 + v^2}{2} + gz + \int_{p_o}^{p} \frac{d\bar{p}}{\rho(\bar{p})} = \frac{q_o^2 + v_o^2}{2} \; ; \tag{4}$$

moist-adiabatic locus of thermodynamic states based on the ground-level state holding at the periphery (previously tabulated and presented here formally),

$$\rho = F(p) \; ; \tag{5}$$

definition of a "mean eyewall pressure",

$$2p = p_{amb} + p_{eye} \; ; \tag{6}$$

and selfconsistency of an isobar in the outer, potential vortex [see Eqs. (11)-(13) below and Appendix C],

$$\tilde{h}(p_{amb}) = \frac{1}{b}[1 - (1 - bz)] \exp\left(-\frac{V_o^2\, R_o^2\, b}{2g\, R^2}\right) . \tag{7}$$

These seven equations are to be solved to yield the dependent variables q, v, p, ρ, p_{amb}, R, and h as functions of the independent spatial variable z(> 0), with the starting conditions at z = 0:

$$R(0) = R_o \, , \frac{dR(0)}{dz} = N \, , \text{given} \, , \tag{8}$$

where we expect N = 0 to be of particular interest. That is, the above equations are taken to hold for an initially vertical updraft, after the throughput has transversed the turnaround, and possibly undergone a "vortex breakdown", in the very-low-altitude subdomain of region III. As yet, we have not studied the selfconsistency of the conditions of Eq. (8) with the behavior holding in the turnaround. In any case, the origin z = 0 is still "close" to ground level. Subscript o denotes known values holding at z = 0. The function $p_{eye}(z)$, which denotes the pressure as a function of altitude z in the central dry, transversely invariant core, is known from preliminary "thermohydrostatic" calculation, as is the tabulated, moist-adiabat-based relationship [Eq. (5)] between ρ and p, the density and pressure, respectively, in the updraft annulus. For completeness, this preliminary set of calculations is summarized in Appendix A.

The (cylindrical-)radial displacement of the "eyewall" from the axis of rotation (and symmetry) is denoted R; the thickness of the "eyewall", h; the swirl speed in the "eyewall", v; the flow speed along the "eyewall", q; the pressure at the interface between the "eyewall" and the outer potential vortex, p_{amb}; and the magnitude of the gravitational acceleration, g. Further, from Appendix A,

$$V_o \approx \left[2(\Delta p) / \rho_o \right]^{1/2} \, , \tag{9}$$

where (Δp) is the near-ground lateral pressure deficit (between the axis of symmetry and the periphery) for a two-cell structure. Also, if q_o is the average radial velocity in the boundary-layer flux, and v_o is the average swirl velocity in the boundary-layer flux,

$$V_o^2 = q_o^2 + v_o^2 \, , \tag{10}$$

a relation obtained in the course of the analysis of the higher-peak-speed, nearer-to-the-axis-of-symmetry portion of the surface frictional layer (Appendix B), in which it is suggested that $q_o \approx v_o$ in the frictional layer near separation. However, q_o (but not v_o) may be decremented in any subsequent vortex breakdown, and the decremented value of q_o would be appropriate for use in Eqs. (1) and (4).

As developed in Appendix C, the swirl in the outer potential vortex is given by [r is recalled to be the (cylindrical-)radial coordinate]

$$v_{outer}^2 = \frac{V_o^2 R_o^2}{r^2} f(z) \, , \tag{11}$$

where at the outset we study the specific case of a linear distribution of the peripheral angular momentum with altitude in the troposphere:

$$f(z) = \beta + (1 - \beta)\left(\frac{z_T - z}{z_T}\right), 0 \le \beta \le 1 . \tag{12}$$

We let

$$f(z) \equiv a - bz , \tag{13}$$

so $a = 1$, $b = (1 - \beta)/z_T$. That is, $\beta = 0$ implies a peripheral swirl so stratified with altitude that no swirl exists at the "lid" $z = z_T$, the known height of the "tropopause"; alternatively, $\beta = 1$ implies a distribution of swirl invariant with altitude. While variation of results with the parameter β is of key interest, we note here, and reiterate below, that if the swirl in the eyewall is smaller that the swirl in the potential vortex near the potential-vortex/eyewall interface, the flow is unstable. Hence, a selfsustaining vortex would not be expected for smaller values of the parameter β.

Eq. (11) links the altitude $\tilde{h}$, at which a particular value of the pressure p_{amb} arises at the periphery, with the (lower) height z at which that same particular value of the pressure p_{amb} holds at the "eyewall"/potential-vortex interface. The function $\tilde{h}(p)$, which gives the height associated with pressure at the periphery, for the peripheral sounding under investigation, is obtained, of course, by hydrostatics from the given data (static temperature and dew-point temperature as a function of pressure).

A factor of 2π has been cancelled from each side of Eq. (1), in which the Taylor entrainment constant $\alpha_E \approx 0.08 - 0.09$ (Turner 1969). While we anticipate entrainment of dry, warm, virtually nonrotating air from the eye into the eyewall, we do not expect much entrainment into the eyewall from the contiguous portions of the potential vortex, especially for those altitudes for which the contiguous-potential-vortex fluid is rotating at a speed in excess of the transversely averaged swirl speed holding in the eyewall. Since the mass entrained into the eyewall is taken to be detrained from the eye, an axial downdrift w_{eye} arises in the eye. If the eye/eyewall interface at altitude z occurs at (cylindrical-)radial distance $[R(z) - h(z)]$, we may estimate the downdrift by the conservation of mass:

$$\rho_{eye}(z)[R(z) - h(z)]^2 w_{eye}(z) = -2 \alpha_E \int_o^z \rho_{eye}(z_1) q(z_1)[R(z_1) - h(z_1)] dz_1 ,$$

where we have taken the downdrift to vanish at the impervious ground plane $z = 0$. We anticipate the downdrift to be comparatively modest, for consistency with the slow recirculatory flow

envisioned for the eye relative to the rapid updraft in the eyewall. The influx into the eye in the upper troposphere is not within the scope of this discussion.

The appearance of the two principal radii of curvature in Eq. (3) may be noted. Equation (3) is to be integrated by: (1) holding the product (ρh) and the difference ($p_{amb} - p_{eye}$) constant over a very small increment in altitude z; (2) using the modified value thus obtained for the "eyewall" radius, R, to update the values for ρ, h, p_{eye}, and p_{amb} at the slightly incremented altitude; and (3) repeating steps (1) and (2) for a further, small increment in altitude, until one attains either the highest altitude, z_T, for which the thermodynamic and dynamic state at the periphery is defined (Appendix A), or until singular behavior intrudes.

We anticipate that, in general, the slope of the eyewall, R_z, is small. If not, then it becomes noteworthy that, whereas all the other dependent variables are functions of the altitude z (as previously stated), in fact the argument of the tabulated function p_{eye} is z', where

$$z' \equiv z + h \frac{R_z}{(1 + R_z^2)^{1/2}} .$$

For completeness, we note that we have regarded the eyewall/potential-vortex interface to be the definition of the displacement R(z), for circumstances in which the nominal smallness of the ratio h/R does not hold.

While the spatial scales R_o and h_o may appear to be independently assignable, in fact, a thin-layer-type, transversely averaged treatment of the eyewall is more appropriate for circumstances for which the ratio $(R_o/h_o) \geq O(10)$. More specifically, the case $(R_o/h_o) = O(10)$ is more plausible under the observation that the mass flux entering the eyewall, $\dot{m}$, is given by

$$\dot{m}_{eyewall} \approx 2\pi \rho_o R_o h_o q_o ; \tag{14}$$

the mass content of the eye, m_{eye}, is given by

$$m_{eye} = \int_0^{z_T} dz \int_0^{R(z)} \rho_{eye}(z)\, 2\pi r\, dr = \pi \int_0^{z_T} R^2(z)\, \rho_{eye}(z)\, dz , \tag{15}$$

where $p_{eye}(z)$ is available from preliminary thermohydrostatic calculation (Appendix A), and R(z) is obtained from solution of the problem posed for the eyewall. If we envision the filling of the eye from throughput detrained from the eyewall during a spin-up stage, which occurs prior to the quasisteady mature stage under examination, then the time $\tilde{T}$ required for such filling is given by

$$\tilde{T} \approx m_{eye} / \dot{m}_{eyewall} . \tag{16}$$

The upper limit z_T in the integral for m_{eye} may be taken to be a somewhat lower value if, as z approaches z_T, the eyewall displacement R slopes appreciably away from the axis of symmetry. (The eye/eyewall structure probably needs re-examination in the form of an outflow-layer analysis for the portion of the flow near the lid.) However, we anticipate that we shall find that the time for filling, $\tilde{T}$, exceeds the observed lifespan of the tornado if R_o far exceeds h_o; if so, such a configuration seems implausible.

4. RESULTS FOR THE ANNULAR ROTATING UPDRAFT

With a preliminary treatment in hand for the eyewall formulation (Section 3) specialized for the turnaround (Appendix D), we now seek results to Eqs. (1)-(16) for the bulk of region III (Fig. 3).

For brevity of reference, we henceforth define the following set of parametric and functional assignments as "the nominal case." The thermohydrostatically derived input z_T, V_o, $p_{eye}(z)$, ρ_o, and $\rho(p)$--the density-pressure relation for the eyewall--is based on the sounding given in Fig. 1; for convenience, we note that $z_T \approx 11.6$ km, $V_o \approx 106.9$ m/s, $\rho_o \approx 1.12$ kg/m^3, $p_{eye}(z)$ is given in Fig. 14, and $\rho(p)$ is given parametrically in terms of the altitude z by Figs. 14 and 16. Since the gravitational acceleration $g = 9.8$ m/s^2 and $v_o = V_o/2^{1/2}$, the remaining quantities to be assigned are β, a dimensionless parameter related to vertical stratification of the peripheral angular momentum [see Eqs. (11)-(13)]; M, a dimensionless parameter related to kinetic-energy loss in the breakdown [see Eq. (B.36)]; N, a dimensionless parameter related to initial eyewall slope [see Eq. (8)]; h_o, the starting thickness of the annulus; and R_o, the starting radial displacement of the eyewall (or equivalent data). For the nominal case, we choose

$$\alpha_E = 0,\ \beta = 0.99,\ M = 2^{1/2},\ N = 0,\ h_o = 35 \text{ m, and } (R_o/h_o) \approx 10\ , \tag{17}$$

where we discuss implications of the last assignment in the next paragraph. Operationally, we find that an integration step size $\Delta z \approx 0.5$ m yields results that are effectively invariant with further refinement of the discretization; with $\Delta z \approx 0.5$ m, solving Eqs. (1)-(16) over $0 \le z \le z_T$ requires roughly 15 min on a 486 PC.

If we let $\varepsilon \equiv R_{zz}(0)$ for brevity of notation, then at $z = 0$, from Eq. (3),

$$\varepsilon h_o = \frac{(1+N^2)^{3/2}}{\rho_o q_o^2/\delta p}\left\{(1+N^2)^{-1/2}\left[\frac{\rho_o v_o^2/\delta p}{R_o/h_o}\right] - 1\right\} \tag{18a}$$

$$\rightarrow \frac{1}{\rho_o q_o^2/\delta p}\left[\frac{\rho_o v_o^2/\delta p}{R_o/h_o} - 1\right] \tag{18b}$$

for the case of primary interest, $N = 0$; $\delta p \equiv p_{amb}(0) - p_{eye}(0)$. Thus, in general, a finite positive (but typically small) curvature exists at $z = 0$. By rearrangement of Eq. (18b),

$$\frac{R_o}{h_o} = \frac{\rho_o v_o^2/\delta p}{\varepsilon h_o\left(\rho_o q_o^2/\delta p\right) + 1}\ . \tag{18c}$$

We see that a smaller (but still positive) value of the nondimensionalized curvature, εh_o, implies a larger value of the ratio (R_o / h_o); in fact, $\varepsilon h_o = 0$ typically implies an appreciably larger value of (R_o / h_o) than that given in Eq. (17), with possible further implications of implausible tornadic structure [recall Eqs. (14) and (15)].

For the nominal case, Fig. 4 presents the radial displacement R(z) and the annular thickness h(z); Fig. 5, the streamwise velocity component q and the swirl v; Fig. 6, the pressure at the potential-vortex/eyewall interface, $p_{amb}(z)$, and the height at the periphery, $\tilde{h}(z)$, at which the pressure $p_{amb}(z)$ occurs; and Fig. 7, the eye mass $m_{eye}(z)$ and the filling time $\tilde{T}$, where the upper limit of the integral Eq. (15) has been changed from z_T to the general value z. The value of the difference $[p_{amb}(z) - p_{eye}(z)]$ is quite small relative to the value of either contribution, and varies from about 500 Pa near an altitude of 1 km to about 300 Pa at 3 km to about 100 Pa at 6 km; the difference goes to zero at about 8.5 km and even very slightly negative above that altitude. The filling time at $z \approx 8.5$ km is about 20 min, but increases rapidly for higher z because the displacement R(z) becomes large at large values of z. The annular thickness h monotonically increases from 35 m at $z = 0$ to about 64 m at 5.8 km, and then monotonically decreases for greater height; correspondingly, the streamwise speed q decreases from 75.6 m/s at $z = 0$ to about 38 m/s at 6.8 km, and then monotonically increases for greater height.

Figures 8 and 10 presents R(z) and h(z), respectively, for several values of the parameter β, all other parameters and functions being held at their nominal values. For the more strongly stratified profiles of the peripheral angular momentum, the eyewall remains very vertical. While a solution may be obtained formally for the strongly stratified case $\beta \rightarrow 0$, its stability warrants investigation. Stability requires that the angular momentum should not decrease with radius, at fixed attitude. Thus the solution is unstable if the inequality $v(z) < v_{outer}[R(z), z]$ holds for any z, where v_{outer} is defined by Eq. (11).

Figures 10 and 11 present R(z) and h(z), respectively, for three values of the parameter h_o, with all other parameters and functions fixed at their nominal values [e.g., $(R_o/h_o) \approx 10$]. Thus, for the nominal case $h_o = 35$ m, $R_o \approx 350$ m (and $\varepsilon \approx 0.002$); for $h_o = 17.5$ m, $R_o \approx 175$ m (and $\varepsilon \approx 0.004$); and for $h_o = 70$ m, $R_o \approx 700$ m (and $\varepsilon \approx 0.001$). Accordingly, the mass flux $\rho_o h_o R_o q_o$ varies by a factor of 16, and the product $R_o v_o$ by a factor of 4, over the three cases. The time $\tilde{T}$ to fill the eye effectively does not vary for these three cases.

Further parametric investigation with the analytic framework already provided, and with the extensions briefly noted in the next section, should permit additional insight into criteria for the existence of selfsustaining intense vortices.

5. CONCLUDING REMARKS

The observable under scrutiny as a possible predictor of tornadogenesis in a mesocyclone is the vertical profile of the angular momentum at the periphery of the mesocyclone. This quantity is closely related to the vertical profile of the circulation, and if indeed the rotation within a tornadic mesocyclone is very roughly that of a potential vortex (except in the core), then the vertical profile of the circulation should be invariant with the lateral distance from the axis at which the profile is measured, for sufficiently large lateral distance. A single sounding is inadequate to obtain the circulation as a function of altitude in the vicinity of a mesocyclone in the atmosphere, and probably futuristic, continuously monitoring, geosynchronous-meteorological-satellite-based wind sensors with vertical resolution would ultimately be required.

Among the future improvements and generalizations of the model is the desirability of smoothing the transition of the total static enthalpy H at the interface of the eyewall (within which $H(z) \approx H_{eo}$) and the potential vortex [with which $H(z) \approx H_e(z)$].

Still another topic warranting further investigation is the upper-tropospheric radial outflow of "processed throughput." In a closed system, this throughput would be compressionally heated as it descended to accommodate the further processing of the convectively unstable fluid of the potential vortex; while evaporative cooling afforded by small-sized condensate carried along by the flow would somewhat counteract the compressional heating, still the descent would partly negate the lightening effected by the presence of an eye. In fact, we believe that there is a high-level lateral efflux of processed air.

However, we particularly emphasize the desirability of seeking further insight into turnaround dynamics by use of a laboratory vortex chamber. A theoretical investigation of the complicated turbulent flow of a compressible fluid in the unconventional geometry of the turnaround would be assisted by experimental verification. Thermodynamics is not at issue in this particular region; inability at laboratory scales to experimentally imitate the moist-air behavior of an atmospheric storm is irrelevant.

APPENDIX A. THERMOHYDROSTATICS FOR A ONE-CELL OR TWO-CELL VORTEX IN CONVECTIVELY-UNSTABLY-STRATIFIED MOIST AIR

A.1 Objectives and Idealizations

By use of (1) the thermodynamics of moist air, (2) the conservation of vertical momentum in the hydrostatic approximation, (3) a sounding (of the static temperature and the dew-point temperature as a function of pressure for a convectively unstable atmosphere), and (4) a simplistic axisymmetric quasisteady model of a one-cell vortex and of a two-cell vortex (Fig. 12), we obtain the thermodynamic states holding within the flow. For a one-cell vortex, fluid at and near the axis of symmetry is described by the locus of thermodynamic states associated with a moist adiabat, based on the ground-level state at the periphery. The associated low-altitude lateral pressure deficit from axis to periphery is relatively modest. For a two-cell vortex, the fluid ascending (nearly vertically) on a moist-adiabatic locus rises in an annulus at a finite radial distance from the axis; the fluid in region IV of Fig. 3 (or Fig. 12) has a locus of thermodynamic states associated with a dry adiabat, based on the thermodynamic state holding at the top of the flow (at all radial distance from axis to periphery). The eye-insertion-associated low-altitude pressure deficit from axis to periphery is relatively large. Since perfectly entrainment-free ascent on a moist adiabat is an idealization, as is slowly recirculatory flow in a perfectly dry eye extending from the top to the bottom of the vortex, the pressure deficits computed for such idealized processes are upper bounds on the corresponding pressure deficits that would be observed for real counterparts of the processes.

The low-altitude peak swirl speed associated with the just-discussed axis-to-periphery pressure deficits may be computed by use of (1) the cyclostrophic approximation to the conservation of angular momentum; (2) an adopted dependence of the swirl on the radial coordinate [the dependence being taken to be a Rankine (combined) vortex for one-cell structure, and a rotationless core patched to a potential vortex for two-cell structure]; and (3) a radial profile for the density [taken to be constant at the ground-level value for the moist-adiabatic column]. As just noted, the lateral pressure deficit is appreciably smaller for a one-cell vortex, and half of the pressure deficit is expended to maintain the rigidly rotating core of a Rankine vortex; thus, the thermohydrostatically derived peak swirl speed for a one-cell vortex is relatively modest, say, 50 m/s or less. The lateral pressure deficit is appreciably greater for a two-cell vortex, and no portion of the deficit need be expended to support rotation of the core, which is virtually nonrotating; thus, the thermohydrostatically derived peak swirl speed for a two-cell vortex is relatively large, say, 100 m/s or more.

There is an altitude at which that total static enthalpy of the near-surface air at the periphery is recovered in the upper troposphere. In fact, we may refer to the height of the lid as the tropopause, though this is by no means the universally standard definition.

A.2 Collection of Standard Relations; Introduction of Notation

If subscripts a and v refer to dry air and water vapor, respectively, then, for convenience of future reference, we recall that the pressure p and the density ρ obey

$$p = p_a + p_v, \rho = \rho_a + \rho_v . \tag{A.1}$$

Also,

$$Y_a \equiv \frac{\rho_a}{\rho}, Y_v \equiv \frac{\rho_v}{\rho}, \text{ so } Y_a + Y_v = 1 \tag{A.2}$$

in the absence of condensed water substance. The equations of state for dry air and water vapor, respectively, if R denotes the gas constant for dry air and σ denotes the ratio of the molecular weight of water vapor to that of dry air,

$$p_a = \rho_a RT, \sigma p_v = \rho_v RT, \text{ so } p - (1 - \sigma) p_v = \rho RT , \tag{A.3a}$$

and

$$Y_v = \sigma p_v / [p - (1 - \sigma) p_v] . \tag{A.3b}$$

The saturation vapor pressure for water is denoted P(T), where a standard excellent curve fit to data (Murray 1967) is given by, with P in Pascals and T in Kelvin,

$$P(T) = 6.1078 \times 10^2 \exp[a(T - 273.16)/(T - b)] , \tag{A.4a}$$

where

$$\left.\begin{matrix} a = 21.8745585 \\ b = 7.66 \end{matrix}\right\} \text{ over ice, } \quad \left.\begin{matrix} a = 17.2693882 \\ b = 35.86 \end{matrix}\right\} \text{ over water .} \tag{A.4b}$$

By definition, the relative humidity RH and the dew-point temperature T_d are related by the following:

$$RH \equiv \frac{p_v}{P(T)} \equiv \frac{P(T_d)}{P(T)} . \tag{A.5}$$

Thus, if the static temperature is given, RH is implied by T_d, and vice versa.

The total static enthalpy H, by definition, is

$$H = c_p T + g z + L Y_v , \tag{A.6}$$

where, in standard notation,

$$c_p = Y_a c_{p_a} + Y_v c_{p_v} \approx c_{p_a} , \tag{A.7}$$

since $(Y_v/Y_a) << 1$ and $c_{p_a}/c_{p_v} = O(1)$ for all the circumstances of interest. [Incidentally, at ground level in warm moist air, $T \approx 300$ K and $(L\, Y_v/c_p) \approx 40$ K; for comparison, if we introduced a total enthalpy (including dynamics), the typical peak tornadic-kinetic-energy contribution $V_o^2/(2\, c_p) \approx 4$ K.]. We also ignore the variation of the specific latent heat L with temperature, and take all condensed water vapor to remain as liquid water (so no heat of freezing is realized).

Finally we recall that, under hydrostatics,

$$\frac{\partial p}{\partial z} = - \rho g , \tag{A.8}$$

so Eq. (A.6) may be written as

$$dH = c_p\, dT - \frac{dp}{\rho} + L\, dY_v . \tag{A.9}$$

For a constant-static-enthalpy process in unsaturated air, so virtually no condensation occurs and $dY_v = 0$, then, with $Y_v \equiv (Y_v)_{ref}$, const.,

$$\frac{dT}{dp} = \frac{1}{\rho c_p} = \frac{RT}{p}\left[1 + \frac{1-\sigma}{\sigma}(Y_v)_{ref}\right] , \tag{A.10a}$$

or, with $(R/c_p) \equiv (\gamma - 1)/\gamma$,

$$\frac{T}{T_{ref}} = \left(\frac{p}{p_{ref}}\right)^{\Upsilon}, \quad \Upsilon \equiv \frac{\gamma - 1}{\gamma}\left[1 + \frac{1-\sigma}{\sigma}(Y_v)_{ref}\right] . \tag{A.10b}$$

The other thermodynamic variables ρ, ρ_v, ρ_a, etc., follow directly. Alternatively, for a constant-static-enthalpy process in saturated air, so RH $\approx$ 1, and $p_v = P(T)$,

$$dY_v = \left\{\sigma\left[P'(T)\right] p\, dT - \sigma P(T)\, dp\right\}/x^2,\ x \equiv p - (1 - \sigma) P(T), \tag{A.11}$$

and

$$\frac{dT}{dp} = \frac{\frac{RT}{x} + \frac{L \sigma P(T)}{x^2}}{c_p + \frac{L \sigma P'(T) p}{x^2}}. \tag{A.12}$$

Again, the other thermodynamic variables follow by straightforward substitution. For $(Y_v)_{ref} = 0$, Eq. (A.10b) describes the locus of thermodynamic states on a "dry adiabat". The locus of states on a "moist adiabat" is described by Eq. (A.10b) prior to saturation (RH < 1), and by Eq. (A.12) after saturation, with the temperature T and pressure p continuous at saturation (RH = 1). In the present approximation, none of the heat is shared with any condensate. Furthermore, even if the condensate is carried along with the gas and exerts no interphase drag on the gas, the condensate is regarded as unavailable for evaporative cooling, so reversal of the process is excluded.

A.3 Thermohydrostatics for a Model of a Vortex in Moist Air

At the periphery of the vortex, i.e., for $r = r_e$ ($>> r_o$), profiles for T(p), and for T_d(p)--or RH(p), are taken as given, often in graphical form (e.g., Fig. 1), typically from a sounding of the atmosphere in "close" proximity, temporally and spatially, to a severe tornado. From straightforward use of Eqs. (A.1)-(A.8), one may obtain all the dependent variables p, p_v, p_a, ρ_v, ρ_a, ρ, T, and H as a function of altitude z, where z = 0 is approximately ground level. In practice, we pursue the dependent variables over a range slightly in excess of $0 \le z \le \tilde{z}_T$, where $H(\tilde{z}_T) = H(0)$; for the convectively unstable sounding of interest, in which a pronounced midtropospheric minimum in H(z) exists (see Fig. 13), z_T = O(10 km). Local anomalies may arise, such that $H(z^*) = H(0)$ for $0 < z^* << 10$ km; such anomalies are ignored in that the sounding is still regarded as convectively unstable overall (even if locally stable), and the value $H(z^*)$ is just an "ordinary" point of the profile. We shall henceforth affix subscript e to indicate that a thermodynamic-variable profile pertains to the vortex periphery.

For the moist-adiabatic locus of thermodynamic states holding for region III, Eq. (A.10b) is used, with the constants $(Y_v)_{ref}$, T_{ref} and p_{ref} associated with $(Y_v)_{eo}$, T_{eo}, and p_{eo}, respectively, where the latter trio are ground-level values holding at the periphery; Eqs. (A.1)-(A.7) are used to associate p_a, p_v, ρ, ρ_a, and ρ_v with p, T, and $(Y_v)_{ref}$, for RH < 1. Upon satisfaction of the condition RH = 1, we use Eq. (A.12) to find T for all higher values of p; in this regime, $p_v = P(T)$,

and the other thermodynamic variables follow as before. Eventually a pair (T,p) on the moist adiabat matches a pair (T_e,p_e) of the sounding; the height at the periphery associated with that particular matching pair (T_e,p_e) is henceforth denoted $z_T(\approx \tilde{z}_T)$, and is adopted as the height of the lid of the storm at all radial positions $0 \le r \le r_e$. Use of hydrostatics [Eq. (A.8)], the tabulated locus of moist-adiabatic states [such that $\rho(p)$ is known], and the known height of the "lid" state permit an altitude z to be associated with each state of the moist-adiabatic locus, until $z = 0$ is reached. The ground-level moist-adiabatic-locus values $p(0)$, $T(0)$, $\rho(0)$, etc., are henceforth denoted p_o, T_o, ρ_o, etc. In general, $p_o < p_{eo}$, with $[(p_{eo} - p_o)/p_{eo}] = O(0.01)$.

Use of hydrostatics, and of Eq. (A.10b) with $(Y_v)_{ref} = 0$, $T_{ref} = T_e(z_T)$, and $p_{ref} = p_e(z_T)$, gives the dry-adiabatic locus of states holding in the eye (region IV):

$$z = z_T - \frac{1}{g}\left(\frac{\gamma}{\gamma - 1}\right)\frac{p(z_T)}{\rho(z_T)}\left\{\left[\frac{p_{eye}(z)}{p(z_T)}\right]^{(\gamma-1)/\gamma} - 1\right\}, \qquad (A.13)$$

where the subscript eye is introduced to distinguish thermodynamic variables holding in a fully inserted, moisture-free eye. At $z = 0$, Eq. (A.13) typically yields a value for $p_{eye}(0)$ such that $[(p_{eo} - p_{eye}(0))/p_{eo}] = O(0.1)$.

An implication of the above treatment, in terms of Fig. 3, is that higher-altitude fluid elements in the potential vortex, although initially characterized by $H < H_{eo}$, during downdrift into the surface layer attain the state $H = H_{eo}$, the ground-level value of the total static enthalpy at the periphery, owing to enthalpy transfer across the ground plane; the total static enthalpy of these fluid elements remains at the value H_{eo} during inflow in the surface layer and ascent in the eyewall. The value $H = H_{eo}$ also characterizes all fluid elements in the eye. If no such cross-boundary enthalpy transfer occurs, the value of H_{eo} decreases slowly in time.

A.4. The Thermohydrostatically Estimated Peak Swirl Speed

In the potential vortex, by conservation of radial momentum,

$$\frac{\partial p}{\partial r} \approx \rho \frac{v_{outer}^2}{r}. \qquad (A.14)$$

We apply Eq. (A.14) near the bottom of the vortex depicted in Fig. 12, and adopt $\rho \approx \rho_o$. For a one-cell vortex (i.e., in the absence of region IV), we adopt the modified Rankine combined-vortex model:

$$v_{outer}(r) = \begin{cases} V_o(r/r_o), & 0 \le r \le r_o \\ V_o(r_o/r)^n, & r_o \le r \le r_e, \end{cases} \qquad (A.15)$$

with $r_e \to \infty$. Substitution of Eq. (A.15) in Eq. (A.14) gives, upon integration,

$$V_o = \left[\left(\frac{2n}{n+1}\right)\frac{p_{eo} - p_o}{\rho_o}\right]^{1/2} . \tag{A.16}$$

For a two-cell vortex (i.e., in the presence of region IV), we adopt:

$$v_{outer}(r) = \begin{cases} 0 , & 0 \le r \le r_o \\ V_o(r_o/r)^n , & r_o \le r \le \infty , \end{cases} \tag{A.17}$$

so

$$V_o = \left[(2n)\frac{p_{eo} - p_{eye}(0)}{\rho_o}\right]^{1/2} . \tag{A.18}$$

In general, in Eqs. (A.16) and (A.18), we limit attention to the case n = 1.

For the sounding of Fig. 1, by use of the formulae presented in this appendix, we compute results presented in Figs. 2 and 13-15. We note that at $z = z_T \approx 11.6$ km, the pressure is about 21.9 kPa; the temperature, about 220 K; the density, about 0.348 kg/m^3; and the total static temperature, H/c_p, about 333 K. The pressure at the base of the sounding, p_{eo}, is about 10^5 Pa; the pressure at the base of the eyewall, p_o, is about 98.7 kPa; the pressure at the base of the eye, $p_{eye}(0)$, is about 93.6 kPa. Since the density at the base of the eyewall, ρ_o, is 1.12 kg/m^3, we compute, for n = 1, that $V_o \approx 33.4$ m/s for a one-cell vortex and $V_o \approx 106.9$ m/s for a two-cell vortex. Incidentally, saturation in the eyewall occurs at $z \approx 2.15$ km, where $p \approx 77.2$ kPa, $p_v \approx 1.39$ kPa, $T \approx 285$ K, and $\rho \approx 0.937$ kg/m^3.

APPENDIX B. ANALYSIS OF THE NEAR-GROUND WIND FIELD FOR AN INTENSE POTENTIAL VORTEX

B.1 Introduction

The velocity field in the near-ground inflow layer (for an incompressible constant-molecular-viscosity fluid) is examined over a closed domain of finite radial extent r_e, where (say) $r_e = 10\, r_o (\equiv R_o)$, r_o being the (given) radius of boundary-layer separation. While the basic results and flowfield structure for the surface boundary layer are long established (Burggraf et al. 1971; Carrier 1971; McWilliams 1971), interest persists (e.g., Phillips and Khoo 1987). Here, convenient approximate expressions, based upon appropriately modified "local similarity" solutions, are presented for the near-ground flow under the high-speed portion of a potential vortex. Conventional eddy-viscosity models for the swirling boundary layer also have been treated in detail (Carrier and Fendell 1977).

In the high-speed portion of the potential vortex, the inward radial pressure gradient is virtually in equilibrium with the centrifugal force (cyclostrophic balance); there is virtually no radial inflow in the well-developed vortex, and there is only a weak downdraft into the surface inflow layer. In the boundary layer, the no-slip boundary conditions retards the centrifugal force, such that a "favorable" pressure gradient drives an appreciable radial influx of swirling air toward the axis of symmetry. Surface friction dissipates some of the angular momentum; in fact, in the boundary layer, well described by the parabolic approximations to the equations for the conservation of radial and azimuthal momentum, the radial velocity component is comparable to, and locally even exceeds, the swirl. Once the radial and azimuthal velocity components are known, the (relatively small) axial velocity component is obtained from continuity.

The overall boundary layer grows monotonically, but rather modestly, in thickness with decreasing radial distance from the axis of symmetry. At larger radial distances from the axis of symmetry, friction plays a role across the entire vertical extent of the near-surface inflow layer. However, closer to the axis, the bulk of the radial inflow is described by inviscid analysis to good approximation; only in a thin sublayer immediately adjacent to the wall does friction alter the radial velocity component significantly, from a near-wall maximum value to zero at the wall (for enforcement of the no-slip boundary condition). The radial velocity component has a larger maximum at smaller radial positions, a maximum that can become as large as the swirl speed above the surface inflow layer at the same radial distance from the axis. On the other hand, the azimuthal-

velocity-component profile is shaped significantly by friction across the entire extent of the surface inflow layer, at all radial positions. At any fixed altitude within the inflow layer, the circulation becomes smaller at smaller radial positions. At a fixed radial distance from the axis, the swirl velocity component decreases monotonically with decreasing altitude above the ground, from its potential-vortex value to zero at the outer edge of the frictional sublayer. Nonoscillatory vertical profiles hold for the radial and axial velocity components, and assertions (e.g., Lewellen 1976) that the swirl within the inflow layer may appreciably exceed its asymptotic value outside the inflow layer, at a fixed radial position, are regarded as unlikely.

The thinning of the frictional sublayer with decreasing radial distance from the axis is consistent with the generally expected behavior of a shear layer that is subject to a favorable (i.e., accelerating) radial pressure gradient; the frictional sublayer is subject to a more rapid radial velocity at its outer edge for smaller radial distances.

In what follows we use these statements to obtain results via numerical integration of very simple ordinary differential equations, rather than via numerical integration of the partial-differential equations (Prahlad and Head 1976; Chi 1977; Shakespeare and Levy 1982).

B.2 Formulation

Under previously discussed approximation, if in cylindrical polar coordinates (r, θ, z) the corresponding velocity components are denoted (u, v, w), the conservation of mass, radial momentum, and angular momentum may be expressed as follows (with subscripts r, z denoting partial differentiation):

$$(r\,u)_r + (r\,w)_z = 0\,; \tag{B.1}$$

$$\frac{(r\,V)^2 - (r\,v)^2 - (r\,u)^2}{r^2} = [v(r\,u)_z]_z - u(r\,u)_r - w(r\,u)_z\,; \tag{B.2}$$

$$[v(r\,v)_z]_z - u(r\,v)_r - w(r\,v)_z = 0\,; \tag{B.3}$$

the boundary conditions are

$$z \to \infty:\ v \to \Gamma/r\,;\ u \to 0\,; \tag{B.4}$$

$$z = 0:\ u = v = w = 0\,; \tag{B.5}$$

$$r = r_e:\ u = 0,\ v \text{ specified } \left(\approx \Gamma/r_e\right). \tag{B.6}$$

Here, r_e is an inferred const., and signifies the radial extent ("edge") of the flow domain. It is anticipated that the formulation is to be applied only in the range $r_0 \le r \le r_e$, where r_0 is the (given,

finite) radius of boundary-layer separation. Also, in the potential vortex, Γ is effectively given, where (with $v_{outer} \equiv V$, for brevity)

$$\Gamma \equiv r\,V = r_o\,V_o, \text{ const.}\,, \tag{B.7}$$

and V_o is inferred from the given peripheral sounding (Appendix A). It may be noted that, as a consequence of standard boundary-layer approximations, the cyclostrophic balance has been used to identify the radial pressure gradient in Eq. (B.2):

$$\frac{1}{\rho}\,p_r = \frac{V^2}{r}\,. \tag{B.8}$$

B.3 Constant-Viscosity Solution

If the kinematic viscosity ν is const., then solution to Eqs. (B.1) - (B.7) is sought in the form [the function $\beta(r)$ is to be distinguished from the parameter β, introduced in Eq. (12)]

$$r\,u = -\Gamma\,\beta(r)\,g'(\eta)\,,\; r\,v = \Gamma f(\eta)\,,\; w = W(\eta)\,, \tag{B.9}$$

where

$$\eta = \frac{z}{[s(r)]^{1/2}}\left(\frac{\Gamma}{\nu}\right)^{1/2}\,. \tag{B.10}$$

The functions s(r) and b(r) are to be identified in solution. One does not expect Eqs. (B.9) and (B.10) to give an exact solution, but to capture the essence of the functional behavior in a very useful form.

Substitution of Eqs. (B.9) - (B.10) in Eq. (B.1) gives

$$\begin{aligned} W_\eta &= (\nu\,\Gamma)^{1/2}\left[\frac{s^{1/2}}{r}\,\beta'\,g' - \frac{\beta\,s'}{2\,r\,s^{1/2}}\,\eta\,g''\right] \\ &= (\nu\,\Gamma)^{1/2}\left[\frac{s^{1/2}}{r}\,\beta'\,g' - \frac{\beta\,s'}{2\,r\,s^{1/2}}\,(\eta\,g' - g)'\right]; \\ &= (\nu\,\Gamma)^{1/2}\left[\left(\frac{s^{1/2}\,\beta'}{r} + \frac{\beta\,s'}{2\,r\,s^{1/2}}\right)g - \frac{\beta\,s'}{2\,r\,s^{1/2}}\,\eta\,g'\right], \end{aligned} \tag{B.11}$$

where, by Eq. (B.5),

$$g(0) = 0. \tag{B.12}$$

Substitution of Eq. (B.9) - (B.10) in Eqs. (B.2) and (B.3) gives, respectively,

$$\frac{\Gamma^2}{r^2}\left(1 - f^2 - \beta^2 g'^2\right) = -\beta\,\Gamma^2\left[\frac{g'''}{s} - \left(\frac{\beta'}{r} + \frac{\beta\, s'}{2\, r\, s}\right) g\, g''\right] - \frac{\Gamma^2}{r}\beta\,\beta'\, g'^2\,; \tag{B.13}$$

$$\Gamma^2\left[\frac{f''}{s} - \left(\frac{\beta'}{r} + \frac{\beta\, s'}{2\, r\, s}\right) g\, f'\right] = 0\,. \tag{B.14}$$

The terms in Eq. (B.13) derive, from left to right, from similarly positioned terms in Eq. (B.2). For self-consistency, one must take

$$\frac{s\,\beta'}{r} + \frac{s'\,\beta}{2\,r} = -1\,, \tag{B.15}$$

say; also, it is necessary, but not sufficient, to take

$$g'^2 = 1 - f^2\,, \tag{B.16}$$

$$\frac{\beta\,\beta'}{r} = -\frac{1 - \beta^2}{r^2}\,. \tag{B.17}$$

From Eq. (B.6), $\beta(r_e) = 0$; hence, from Eq. (B.17),

$$\beta^2 = \frac{r_e^2 - r^2}{r_e^2}\,. \tag{B.18}$$

Equation Eq. (B.15) may be written

$$\left(\beta^2\, s\right)' = -2\, r\, \beta \Rightarrow s = \frac{2}{3}\, r_e \left(r_e^2 - r^2\right)^{1/2} \tag{B.19}$$

by use of Eq. (B.18).

The term in square brackets in Eq. (B.13) is $O(\beta\Gamma^2/s)$, while the other terms are $O(\Gamma^2/r^2)$; substitution of Eqs. (B.18) and (B.19) shows that the ratio of the bracketed to unbracketed terms is $O\left[(3\, r^2)/(2\, r_e^2)\right]$, so that, for $r << r_e$, the bracketed term is negligible. The neglect of the bracketed term gives an inaccurate result where the motion is slow [i.e., where $v = O(v_{max}/10)$, $u < O(v_{max}/10)$], and an accurate result where the motion is fast. From Eq. (B.19), $s^{1/2} \sim (r_e - r)^{1/4}$, as $r \rightarrow r_e$; this is consistent with the more meticulous analysis of Stewartson, Burggraf, and Belcher (1971). The flow structure remains less evident in other approaches (e.g., Kuo 1971, 1982).

The radial momentum equation for $r_e^2 >> r^2$, so that $\beta \rightarrow 1$, becomes a statement that the left-hand side of Eq. (B.2) vanishes; i.e., $V^2 = u^2 + v^2$, such that the radial velocity component is

inviscidly controlled. The two-point nonlinear third-order boundary-value problem, from Eqs. (B.13) - (B.16), becomes

$$f''' + g\,f' = 0\,; \tag{B.20}$$

$$g' = \left(1 - f^2\right)^{1/2}\,; \tag{B.21}$$

$$f(0) = g(0) = 0,\ f\left(\infty\right) \to 1\,. \tag{B.22}$$

The boundary conditions follow from Eqs. (B.4), (B.5), (B.7), (B.9), (B.10), and (B.12). The problem is readily solved numerically by shooting; one finds

$$f'(0) \doteq 0.7456,\ g\left(\infty\right) \doteq 1.941\,. \tag{B.23}$$

Results are graphed in Figs. 17 and 18, where it is evident that f monotonically increases as η increases (so g′ monotonically decreases). Note that $g'(0) = 1$ (cf. Rotunno 1980).

Of course, the reduction to third order results from dropping of the frictional term in the conservation of radial momentum Eq. (B.3), which has been taken in the inviscid form Eq. (B.16). Enforcement of all of Eq. (B.5), specifically $g'(0) = 0$ so that $u(x, z = 0) = 0$, requires restoration of the frictional term in a thin near-wall sublayer of the inflow layer.

For completeness, a brief sketch of the near-wall sublayer, in which u falls to zero, is developed now. If [with the dimensionless function $h(\sigma)$ introduced here to be distinguished from the eyewall thickness h(z), introduced in the main text]

$$r\,u = -\,\Gamma\,\beta(r)\,h'(\sigma)\,,\ \sigma = \frac{z}{m(r)}\left(\frac{\Gamma}{\nu}\right)^{1/2}\,,\ \beta = 1 - (r/r_e)^2\,, \tag{B.24}$$

then from continuity

$$(r\,w)_\sigma = m\left(\frac{\nu}{\Gamma}\right)^{1/2}\left[\beta'\,\Gamma\,h' - \beta\,\Gamma\,h''\left(\frac{m'}{m}\right)\sigma\right], \tag{B.25}$$

or

$$(r\,w) = m\left(\frac{\nu}{\Gamma}\right)^{1/2}\left[\beta'\,\Gamma\,h - \beta\,\Gamma\left(\frac{m'}{m}\right)\left(\sigma\,h' - h\right)\right]. \tag{B.26}$$

From the radial momentum equation,

$$-\left(\frac{\beta}{m^2}\right)h''' - \left(\frac{\beta\,\beta'}{r}\right)h'^2 + \left[\frac{\beta\left(\beta' + \beta m^{-1}\,m'\right)}{r}\right]h\,h'' = \frac{1}{r^2} - \left(\frac{\beta^2}{r^2}\right)h'^2 + \left(\frac{1}{r^2}\right)f^2\,, \tag{B.27}$$

where the last term involving f^2 is dropped as negligible. The function m is assigned by demanding

$$\frac{\beta^2 m'}{r m} = \frac{1}{r^2} . \tag{B.28}$$

If attention is concentrated on $(r/r_e) << 1$, such that $\beta \rightarrow 1, \beta' \rightarrow o(1)$, then

$$m \doteq r , \tag{B.29}$$

and

$$- h''' + (h h')' \doteq 1 , \tag{B.30}$$

where all neglected terms are $O(r^2/r_e^2)$ or smaller. The boundary conditions are

$$h(0) = 0 , h'(0) = 0 , h'(\infty) \rightarrow 1 ; \tag{B.31}$$

these enforce $w(x,z = 0) = 0$, $u(x,z = 0) = 0$, and matching of the sublayer and outer-layer solutions, respectively. One arrives at a Riccati equation

$$- h' + \frac{h^2}{2} = \frac{\sigma^2}{2} - h''(0)\,\sigma , h(\sigma \rightarrow \infty) \rightarrow \sigma , \tag{B.32}$$

where the boundary conditions conditions have been used to assign a constant of integration. The results of Burggraf, Stewartson, and Belcher (1971) assure that a solution exists, and for present purposes

$$h(\sigma) \doteq \sigma + \exp(-\sigma) - 1 \Rightarrow h'(\sigma) = 1 - \exp(-\sigma) , \tag{B.33}$$

captures its behavior adequately (see Fig. 19). Hence, a uniformly valid expression for $r^2 << r_e^2$ is

$$r u \doteq - \Gamma \beta(r)[h'(\sigma) + h'(\eta) - 1] , \tag{B.34}$$

where $h'(\sigma)$ is given by Eq. (B.32), or , facilely, by Eq. (B.33), and $h'(\eta)$ is given by Eqs. (B.20) - (B.22).

This modification to encompass the sublayer is regarded here as a detail from an engineering point of view; the solution to Eqs. (B.20) - (B.22) would normally furnish an adequate approximation by itself. However, completion of the surface-inflow-layer analysis does emphasize the compatibility of separated-inflow-layer properties with the properties of contiguous eye air on one side of the annulus, and with the properties of the contiguous potential-vortex fluid on the other side. The fluid in the nonrotating sublayer of the inflow becomes contiguous to the

nonrotating, slowly recirculating air of the eye. The rapidly rotating fluid of the outer layer of the inflow becomes contiguous to the rapidly rotating air of the potential vortex, and exerts very little streamwise shear on the potential-vortex air.

B.4 Pertinence of the Surface-Inflow-Layer Solution

The quantities q_o and v_o in Eqs. (4) and (8) are transversely averaged values (of the streamwise and swirl velocity components, respectively) holding at $z = 0$, the bottom of the eyewall, where the height $z = 0$ is after the turnaround. If the kinetic energy is conserved through the turnaround, then the relation $V^2 = u^2 + v^2$, given just above Eq. (B.20), suggests the relation $V_o^2 = q_o^2 + v_o^2$, where, at separation of the surface-inflow layer, the streamwise-velocity component q^2 is identical with the radial inflow u^2. We adopt, at a fixed value of $r << r_e$, a flux-weighted transverse average of the radial-inflow velocity component u and of the swirl component v, for the purpose of establishing the value of the ratio (q_o/v_o):

$$\frac{q_o}{v_o} = \frac{2\pi r\rho \int_o^\infty u^2\, dz}{2\pi r\rho \int_o^\infty |u|\, v\, dz} = \frac{\int_o^\infty (1 - f^2)\, d\eta}{\int_o^\infty f(1 - f^2)^{1/2}\, d\eta}, \qquad \text{(B.35)}$$

by use of Eqs. (B.9), (B.10), and (B.21). Attention is confined entirely to the major, inviscid portion of the inflow layer, described implicitly by the solution of Eqs. (B.20) - (B.22). Substitution of the numerically derived solution for $f(\eta)$ in Eq. (B.35) gives $(q_o/v_o) \approx 1.07$, or, approximately, $q_o \approx v_o$. If this relation between q_o and v_o continues to hold through the turnaround, Eq. (8) may be written as $V_o^2 = q_o^2 + v_o^2 \doteq 2q_o^2 \doteq 2v_o^2$. More generally, the streamwise velocity component may be decremented owing to a vortex breakdown in the turnaround, whereas the conservation of angular momentum plausibly holds across the turnaround, so v_o remains unaltered. Thus, in general,

$$q_o = \frac{V_o}{M},\ v_o = \frac{V_o}{2^{1/2}} \Rightarrow q_o^2 + v_o^2 = V_o^2\left(\frac{1}{2} + \frac{1}{M^2}\right) \le V_o^2\,, \qquad \text{(B.36)}$$

where $M(\ge 2^{1/2})$ is a factor to be assigned for parametric investigation in view of the limited understanding of the "breakdown" of an annular column with swirling flow.

A motivation for regarding an abrupt deceleration of the streamwise flow in the swirling-updraft annulus as plausible is provided by the dust striations recorded in certain tornado photographs [e.g., of the June 5, 1966 tornado at Enid, OK (see Gwynne 1982, p. 55; Lugt 1983,

p. 192)], and by examining the results of photogammetry carried out for a few tornadoes (Grazulis 1991, pp. 100-101). Under the approximation that the interphase velocity slip between the observed particles and the colocated air is negligible, we note that, for the low-altitude, near-core flow in the tornado, the angle of the velocity vector for the fluid with respect to the ground plane typically tends to be appreciably less than 45°. Thus, the inequality $v > q$ is inferred in the post-turnaround flow from photographic data, although $v \approx q$ at separation of the surface inflow layer, from the above analysis. This would be consistent with a nonentraining vortex transition (with conversion of mechanical energy to heat) in the turnaround region.

APPENDIX C. THE SELFCONSISTENT VORTICAL FIELD OUTSIDE THE EYEWALL

Derivation of Eq. (7) involves examination of the isobars in region I, the outer potential vortex, holding for $R(z) \le r \le \infty$ (for $r_e \to \infty$). Under the cyclostrophic and hydrostatic approximations, appropriate for region I,

$$p_r = \rho v_{outer}^2 / r \,, \tag{C.1}$$

$$p_z = -\rho g \,, \tag{C.2}$$

where the notation is standard (except that we emphasize by subscript that the relevant swirl pertains to the potential-vortex region only). On an isobar,

$$dp = p_r \, dr + p_z \, dz = 0 \,, \tag{C.3}$$

or

$$\frac{dr}{dz} = - \frac{p_z}{p_r} = \frac{gr}{v_{outer}^2} \,. \tag{C.4}$$

Under the family of spin-up states specified by Eqs. (11) and (12),

$$V_o^2 R_o^2 \int_r^\infty \frac{d\theta}{\theta^3} = g \int_{z(r;p)}^{z(\infty;p)} \frac{d\phi}{f(\phi)} \,. \tag{C.5}$$

For the linear profile for f(z) given in Eqs. (13),

$$\frac{V_o^2 R_o^2}{2r^2} = \frac{g}{b} \ln \left[\frac{a - b \, z(r;p)}{a - b \, \tilde{h}(p)} \right] , \tag{C.6}$$

where $a = 1$, $b = (1 - \beta)/z_T$, and $0 \le \beta \le 1$, with z_T obtained from Appendix A and with β specified as a parametric input. The pressure p takes on the value for which the integration is performed; $z(\infty;p)$ is the height of the isobar for pressure p at the periphery of the storm; and $z(r;p)$ is the height of the same isobar at some finite cylindrical-radial distance from the axis. We henceforth denote $z(\infty;p)$ as $\tilde{h}(p)$, the altitude at which the unspun periphery has the pressure p according to results of Appendix A. (The tilde is present because symbol h has been preempted for another quantity.) If we let $r = R(z)$, the locus of the eyewall displacement, then

$$\frac{V_o^2 R_o^2}{2R^2(z;p)} = \frac{g}{b} \ln \left[\frac{1 - b \, z(R;p)}{1 - b \, \tilde{h}(p)} \right] , \tag{C.7}$$

where the pressure p at r = R is denoted p_{amb}. By rearrangement, we obtain Eq. (7), explicitly,

$$\tilde{h}(p_{amb}) = \frac{1}{b}\left[1 - (1 - bz)\exp\left(-\frac{b\,V_o^2\,R_o^2}{2\,g\,R^2}\right)\right]. \qquad (C.8)$$

Upon fixing the parameter b, each pair of values for z and R implies a value for $\tilde{h}(p_{amb})$, and, then, by interpolation in the thermohydrostatic tables, p_{amb}. For example, at $z \approx 0$, where $R = R_o$, $\tilde{h} = \{1 - \exp[-b\,V_o^2/(2g)]\}/b$, so $\tilde{h} > 0$. As expected, the isobars dip groundward as the radial distance from the axis of rotation decreases; only for $R^2 >> (b\,V_o^2\,R_o^2)/2g$ does $\tilde{h}(p_{amb}) \rightarrow z$, the height of the isobar at the eyewall/potential-vortex interface. Since thermohydrostatic results typically are not tabulated for altitudes above z_T, tabulated values for $\tilde{h}$ may be exhausted before the top of the eyewall is attained in the integration described in Section 3.

If, instead of the linear relation for f(z) given by Eq. (13), we adopt the two-part expression (say, $0 \le \beta_2 \le 0.3$)

$$f(z) = \begin{cases} 1, & 0 \le z \le z_1 \\ 1 - \beta_2\left(\dfrac{z - z_1}{z_T - z_1}\right)^2, & z_1 \le z \le z_T, \end{cases} \qquad (C.9)$$

where (for the sake of an explicit choice) z_1 may be taken to be the altitude at which the eyewall becomes saturated. Substitution of Eq. (C.9) in Eq. (C.5) gives, for r = R(z),

$$\tilde{h}(p_{amb}) = z + \frac{V_o^2\,R_o^2}{2\,g\,R^2},\ 0 \le z \le \tilde{h} \le z_1\ ; \qquad (C.10a)$$

$$\frac{\tilde{h}(p_{amb}) - z_1}{z_T - z_1} = \frac{1}{\beta_2^{1/2}}\frac{1 - Q}{1 + Q}, \qquad (C.10b)$$

where, if $\delta_2 \equiv \beta_2^{1/2}[(z - z_1)/(z_T - z_1)]$,

$$Q \equiv \begin{cases} \exp\left\{-\dfrac{2\beta_2^{1/2}}{z_T - z_1}\left[\dfrac{V_o^2\,R_o^2}{z\,g\,R^2} + (z - z_1)\right]\right\}, & z \le z_1 \le \tilde{h} \le z_T \\ \dfrac{1 - \delta_2}{1 + \delta_2}\exp\left[-\dfrac{\beta_2^{1/2}\,V_o^2\,R_o^2}{g(z_T - z_1)\,R^2}\right], & z_1 \le z \le \tilde{h} \le z_T. \end{cases} \qquad (C.10c)$$

APPENDIX D. THE TURNAROUND

We consider the very-low-level portion of region III, in which the surface-inflow layer separates and "overshoots" its equilibrium position, owing to dynamic forces; consequently, in the "overshoot", under conservation of angular momentum, the local swirl speed may modestly exceed the thermohydrostatically computed peak value V_o. Eventually, restorative forces result in an "overcompensatory" locus for the lower eyewall, such that the local swirl speed may "undershoot" its equilibrium value. In fact, an endless cycle of overshooting and undershooting behavior is formally obtained as the solution for the formulation (for the turnaround), which is translationally invariant in the independent variable (the altitude z). The limit-cycle behavior is of purely academic interest because: (1) the translationally invariant formulation is inadequate (because, inter alia, change of the eye pressure and of the gravitational potential energy with altitude cannot be justifiably ignored), and, far more importantly, (2) the flow is likely to be unstable to breakdown in view of the centrifugal forces acting in a flow with curved streamlines. Vortex-breakdown theory (Hall 1972; Leibovich 1976) pertains to axis-enveloping swirling flow (with a stagnation point on the axis), often (but not always) confined in a tube; the annular geometry of relevance here is largely uninvestigated. Nevertheless, although we can provide no quantification, the existence of a breakdown is highly plausible. We proceed with an analysis of the turnaround to confirm that the equations and boundary conditions yield solutions consistent with the just-described anticipations.

Equations (1) - (3) and (6) are unaltered from those given earlier, but Eq. (7) is modified because we take $\rho \approx \rho_o$ in the very low portion of the potential vortex, and we adopt the entrainment-free ($\alpha_E = 0$) form of Eq. (1). Then, if v_{outer} denotes the swirl speed in the potential vortex,

$$\frac{\partial p}{\partial r} = \rho_o \frac{v_{outer}^2}{r} = \rho_o \frac{V_o^2 R_o^2}{r^3}; \tag{D.1}$$

hence, in the potential vortex,

$$p = -\frac{\rho_o V_o^2}{2}\left(\frac{R_o^2}{r^2}\right) + \text{const}. \tag{D.2}$$

At the separating-layer/potential-vortex interface, $r \rightarrow R$ and $p \rightarrow p_{amb}$, by definition:

$$p_{amb} = -\frac{\rho_o V_o^2}{2}\left(\frac{R_o^2}{R^2}\right) + \text{const}. \tag{D.3}$$

If the frictional layer separates smoothly (the particular case to be examined here), since the pressure is invariant, to lowest order of approximation, across a thin near-wall layer under the classical arguments of Prandtl, then $p_{amb} = p_{eye}$ for $R = R_o$ (see Fig. 3). Under this assignment for the constant of integration,

$$p_{amb} - p_{eye} = \frac{\rho_o V_o^2}{2}\left(1 - \frac{R_o^2}{R^2}\right) = \rho_o q_o^2\left(1 - \frac{R_o^2}{R^2}\right), \tag{D.4}$$

where the last equality arises from the fact that Eq. (9) may be rewritten (Appendix B) as

$$V_o^2 = q_o^2 + v_o^2 \approx 2q_o^2 \approx 2v_o^2 , \tag{D.5}$$

prior to the occurrence of any possible breakdown phenomenon. The above derivation implies that the potential-vortex behavior describes the swirl across the separating inflow layer.

Bernoulli's equation [Eq. (4)] becomes, upon neglect of the gravitational potential energy, under Eqs. (6), (D.4) and (D.5),

$$\frac{v^2 + q^2}{2} + \int_{p_{eye}}^{p} \frac{dp'}{\rho(p')} = \frac{q_o^2 + v_o^2}{2}, \quad \text{where } p = p_{eye} + \frac{\rho_o q_o^2}{2}\left(1 - \frac{R_o^2}{R^2}\right) \tag{D.6}$$

from Eqs. (6) and (D.4). Since $v^2 = q_o^2 R_o^2/R^2$, and since $\rho(p)$ is tabulated from preliminary hydrostatics, Eq. (D.6) provides an expression for (q/q_o) as a function of (R/R_o).

We adopt the following nondimensionalization and parameter definition:

$$\bar{R} \equiv \frac{R}{R_o}, \ \bar{z} \equiv \frac{z}{R_o}, \ \bar{\rho} \equiv \frac{\rho}{\rho_o}, \ \bar{h} \equiv \frac{h}{h_o}, \ \bar{p} \equiv \frac{p}{p_{eye}},$$

$$\bar{q} \equiv \frac{q}{q_o}, \ \bar{v} \equiv \frac{v}{q_o}, \ \alpha \equiv R_o/h_o, \ \Upsilon \equiv \frac{2\,p_{eye}}{\rho_o q_o^2}, \tag{D.7}$$

so

$\bar{\rho}\,\bar{h} = (\bar{q}\,\bar{R})^{-1}$, $\bar{v} = (\bar{R})^{-1}$, and

$$\bar{R}_{\bar{z}\bar{z}} = \frac{1 + (\bar{R}_{\bar{z}})^2}{\bar{R}^2\,\bar{q}[\bar{R};\Upsilon]}\left\{\frac{1}{\bar{R}} \pm \alpha\,\bar{R}(\bar{R}^2 - 1)\left[1 + (\bar{R}_{\bar{z}})^2\right]^{1/2}\bar{q}[\bar{R};\Upsilon]\right\}, \tag{D.8}$$

where

$$\bar{q}[\bar{R};\Upsilon] = \left\{ \frac{2\bar{R}^2 - 1}{\bar{R}^2} - \Upsilon F\left[\Upsilon^{-1}\left(\frac{\bar{R}^2 - 1}{\bar{R}^2} \right) \right] \right\}^{1/2} , \tag{D.9}$$

$$F(x) \equiv \int_1^{1+x} \frac{d\bar{p}'}{\bar{\rho}(\bar{p}')} . \tag{D.10}$$

Since we anticipate that $\bar{R}_{\bar{z}} \to \pm\infty$ within the domain of integration, it is locally convenient to interchange the roles of dependent and independent variables, so $\bar{R}(\bar{z}) \to \bar{z}(\bar{R})$:

$$\bar{R}_{\bar{z}} = (\bar{z}_{\bar{R}})^{-1} , \bar{R}_{\bar{z}\bar{z}} = - \frac{\bar{z}_{\bar{R}\bar{R}}}{(\bar{z}_{\bar{R}})^2} . \tag{D.11}$$

Hence,

$$\bar{z}_{\bar{R}\bar{R}} = \frac{1 + (\bar{z}_{\bar{R}})^2}{\bar{R}^2 \bar{q}[\bar{R};\Upsilon]} \left\{ - \frac{\bar{z}_{\bar{R}}}{\bar{R}} \pm \alpha \bar{R}(\bar{R}^2 - 1)[1 + (\bar{z}_{\bar{R}})^2]^{1/2} \bar{q}[\bar{R};\Upsilon] \right\}^{1/2} . \tag{D.12}$$

The symbol ± before the term containing a square root implies that we may choose the physically pertinent branch of the root, i.e., the physically pertinent curvature.

Starting conditions, holding at the position of the surface-inflow-layer separation, are taken to be those for a smooth separation:

$$\bar{z} = 0, \bar{R} = 1, \bar{z}_{\bar{R}} = 0 , \tag{D.13}$$

such that Eq. (D.12) is convenient for the initial incursion $(\bar{R} < 1)$ of the separated layer, until $\bar{z}_{\bar{R}}$ becomes large. Then, with continuity of the values of $\bar{z}$, $\bar{R}$, and $\bar{z}_{\bar{R}} \left[\equiv (\bar{R}_{\bar{z}})^{-1} \right]$ at a convenient point of transition (say, $|\bar{z}_{\bar{R}}| = 1$), we adopt Eq. (D.8) to proceed to $\bar{R} = \bar{R}_{min}$ and continue on until $\bar{R} \to 1$ and $\bar{R}_{\bar{z}} \to \infty$, so we revert to the use of Eq. (D.12) to begin the subsequent excursion $(\bar{R} > 1)$, etc. If we denote Eq. (D.8) as formulation I and Eq. (D.12), formulation II, then Fig. 20 indicates which formulation is convenient for various portions of the incursion/excursion cycle; Fig. 20 also indicates which trial-and-error choice of sign for the square root is physically appropriate, where the choice of sign in formulation I may be switched across a point at which $|\bar{z}_{\bar{R}}| \to \infty$, i.e., across $\bar{R} = \bar{R}_{min}$ (< 1) and $\bar{R} = \bar{R}_{max}$ (> 1), and, correspondingly, the choice of sign in formulation II may be switched across a point at which $|\bar{R}_{\bar{z}}| \to \infty$, i.e., across $\bar{R} = 1$.

Results are presented in Fig. 21 for the physically interesting parameter values $\alpha = 5$ and 10, $\Upsilon \approx 29.4$, under the following curve fit to thermohydrostatic tabulations for the lower portions of the moist adiabat for a specific sounding (Figs. 1 and 2) of a tornado-proximity atmosphere (Appendix A):

$$\overline{\rho}(\overline{p}) \approx 0.0654 + 1.066\,\overline{p} - 0.1663\,\overline{p}^2 \qquad \text{(D.14)}$$

over the range of $\overline{p}$ of interest, explicitly, $\overline{p} = O(1)$. Since $\overline{v} = (\overline{R})^{-1}$, in view of Eqs. (D.5) and (D.7), the value of $(2^{1/2}\,\overline{R}_{min})^{-1}$ gives the ratio of the peak swirl to the nominal, thermohydrostatically computed peak swirl, V_o, for a specific (but typical) case. This very local increase in the swirl over the value V_o is termed the "overshoot". All the dependent variables may be straightforwardly deduced from knowledge of $\overline{R}(\overline{z})$, but these details are not pursued. We anticipate that a breakdown occurs on the first occasion in the turnaround for which an incursion of the separated inflow layer undergoes transition to an excursion, but we are highly uncertain about the details.

Acknowledgements

The authors are grateful to Steven Goodman and Eugene McCaul of NASA Marshall Space Flight Center for helpful guidance concerning sensors, especially concerning atmospheric-wind-measuring instrumentation, and to John Theon of NASA Headquarters for encouraging this investigation. The authors wish to thank Gail Takahashi for preparation of the manuscript.

References

Brown, R. A. (1987). Severe thunderstorms (meteorology). Encyclopedia of Physical Science Technology, ed. by R. A. Meyers, Academic, New York, NY, Vol. 12, 554-570.

Burggraf, O. R., Stewartson, K., and Belcher, R. (1971). Boundary layer induced by a potential vortex. Phys. Fluids 14, 1821-1833.

Carrier, G .F. (1971). Swirling flow boundary layers. J. Fluid Mech. 49, 133-144.

Carrier, G. F., and Fendell, F. E. (1977). Analysis of the near-ground wind field of a tornado. Report 29584-6001-RU-00, TRW Defense and Space Systems, Redondo Beach, CA, 43 pp.

Carrier, G. F., Fendell, F. E., Feldman, P. S., and Fink, S. F. (1984). Conditions for two-cell structure in severe vortical storms. Report 35524.6003-UT-00, TRW Space and Technology Group Redondo Beach, CA, 104 + vi pp.

Chi, J. (1977). Numerical analysis of turbulent end-wall boundary layers of intense vortices. J. Fluid Mech. 82, 209-222.

Dergarabedian, P., and Fendell, F. (1970). On estimation of maximum wind speeds in tornadoes and hurricanes. J. Astronaut. Sci. 17, 218-236.

Dergarabedian, P., and Fendell, F. E. (1971a). Estimation of maximum wind speeds in tornadoes. Tellus 22, 511-516.

Dergarabedian, P., and Fendell, F. E. (1971b). A method for rapid estimation of maximum tangential wind speed in tornadoes. Mon. Wea. Rev. 99, 143-145.

Dergarabedian, P., and Fendell, F. E. (1977). One-and two-cell structure in tornadoes. Proceedings of the Symposium on Tornadoes: Assessment of Knowledge and Implications for Man, Institute for Disaster Research, Texas Tech. U., Lubbock, TX, 501-521.

Fendell, F. E. (1974). Tropical cyclones. Advances in Geophysics 17, 1-100.

Grazulis, T. P. (1991). Significant Tornadoes, 1880-1898. Vol. 1: Discussions and Analysis, Environmental Films, St. Johnsbury, VT.

Gwynne, P. (1982). Looking into tornadoes. Audubon 84 (2, March), 44-45.

Hall, M. G. (1972). Vortex breakdown. Ann. Rev. Fluid. Mech. 4, 195-217.

Kuo, H. L. (1971). Axisymmetric flows in the boundary layer of a maintained vortex. J. Atmos. Sci. 21, 20-41.

Kuo, H. L. (1982). Vortex boundary layer under quadratic surface stress. Boundary Layer Meteor. 22, 152-169.

Leibovich, S. (1978). The structure of vortex breakdown. Ann. Rev. Fluid Mech. 10,.221-246.

Lewellen, W. S. (1976). Theoretical models of the tornado vortex. Proceedings of the Symposium on Tornadoes: Assessment of Knowledge and Implications for Man, Institute for Disaster Research, Texas Tech U., Lubbock, TX, 107-143.

Lugt, H. J. (1983). Vortex Flow in Nature and Technology, John Wiley, New York, NY.

Maxworthy, T. (1972). The laboratory modelling of atmospheric vortices: a critical review. Intense Atmospheric Vortices, ed. by L. Bengtsson and M. J. Lighthill, Springer-Verlag, New York, NY, 229-246.

McWilliams, J. C. (1971). The boundary layer dynamics of symmetric vortices. Ph.D. thesis, Harvard University, Cambridge, MA.

Murray, F. J. (1967). On the computation of saturation vapor pressure. J. Appl. Meteor. 6, 203-204.

Phillips, W. R. C., and Khoo, D. C. (1987). The boundary layer beneath a Rankine-like vortex. Proc. R. Soc. Lond. A411, 177-192.

Prahlad, T. S., and Head, M. R. (1976). Numerical solutions for boundary layers beneath a potential vortex. Computers and Fluids 4, 157-169.

Rotunno, R. (1980). Vorticity dynamics of a convective swirling boundary layer. J. Fluid Mech. 97, 623-640.

Rotunno, R. (1986). Tornadoes and tornadogenesis. Mesoscale Meteorology and Forecasting, ed. by P. S. Ray, Amer. Meteor. Soc., Boston, MA, 414-436.

Shakespeare, W. J., and Levy, E. K. (1982). Laminar boundary layer near the rotating end wall of a confined vortex. J. Fluids Engineering 104, 171-177.

Turner, J. S. (1969). Buoyant plumes and thermals. Ann. Rev. Fluid Mech. 1, 29-44.

Walko, R. L. (1988). Plausibility of substantial dry adiabatic subsidence in a tornado core. J. Atmos. Sci. 45, 2251-2267.

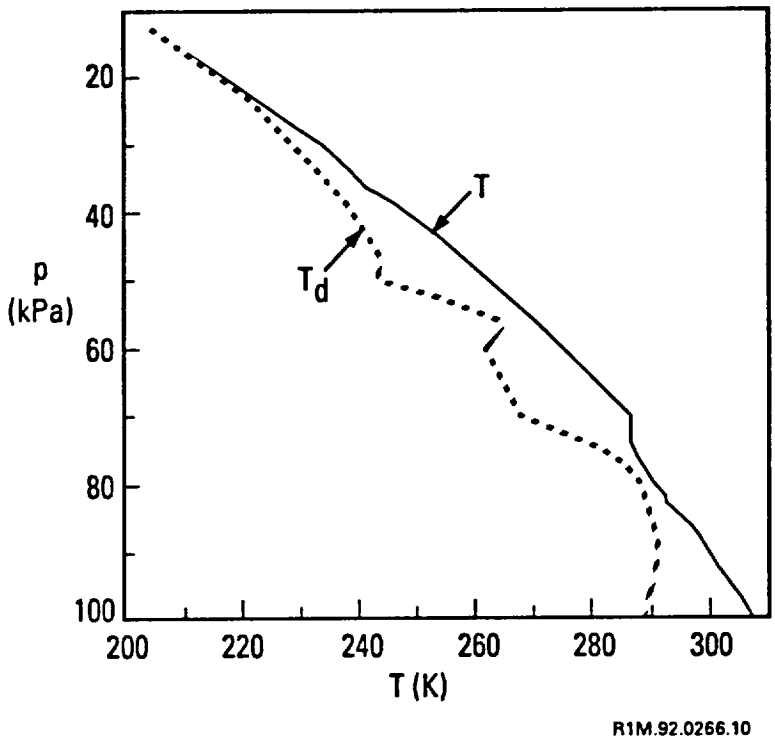

Fig. 1. Convectively unstable sounding (with a moderately large midtropospheric minimum in the total static enthalpy), measured in the vicinity of a tornado at Jackson, MS on April 17, 1978 at 2300Z. The static temperature is T; the dew-point temperature, T_d; the pressure, p.

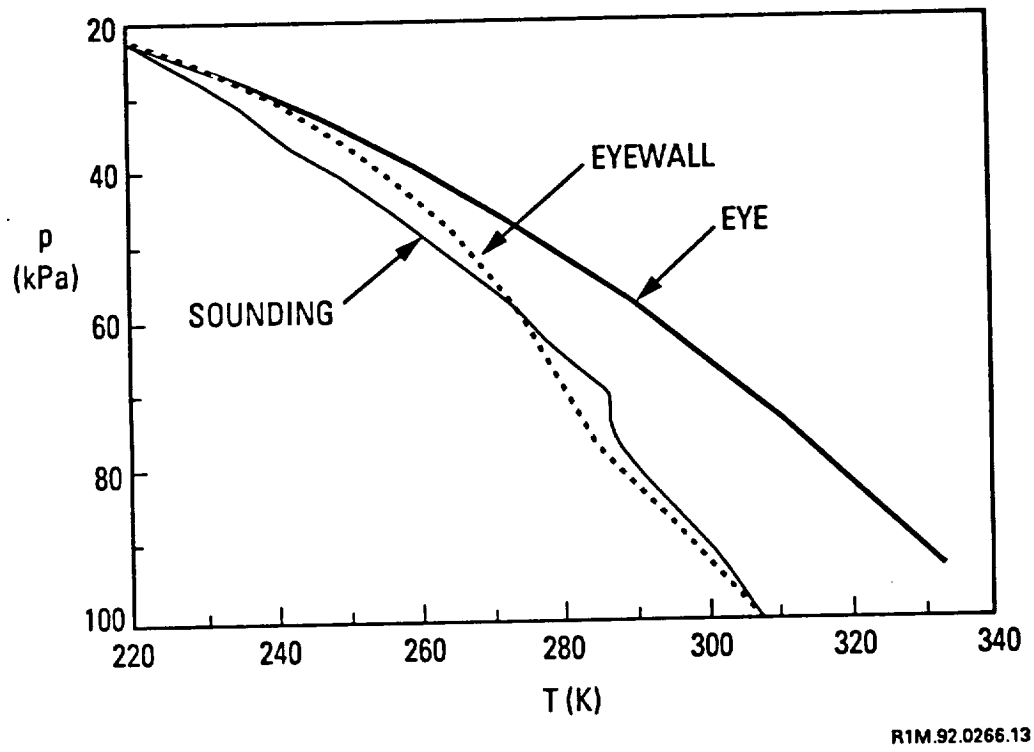

Fig. 2. Pressure-temperature relations for the sounding of Fig. 1 (circles); for ground-level air raised on a moist adiabat to its level of neutral stability, at which its density is equal to that of the air of the sounding (triangles); and for neutral-stability-altitude air compressed dry-adiabatically to ground level (diamonds).

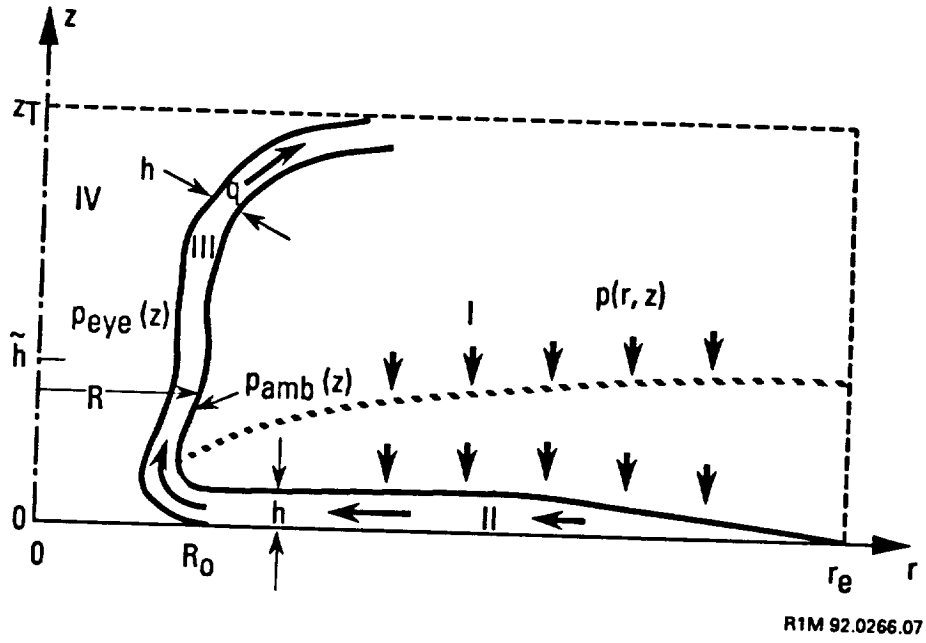

Fig. 3. Schematic of a postulated four-part model of the structure of a quasisteady two-cell vortex, of axial extent z_T (the "lid" of the storm). Region I is the outer potential vortex; II, the near-ground inflow layer; III, the "eyewall", the lowest portion of which is termed the turnaround; and IV, the "eye". The dotted curve is a sketched isobar, which is at altitude $\tilde{h}$ at the periphery, $r \rightarrow r_e$, and at lower altitude at the "eyewall"/potential-vortex interface, $r = R(z)$, with $R(0) \equiv R_0$ and $r_e >> R_0$. The arrows schematically indicate the magnitude and direction of the secondary (i.e., radial and axial) flow.

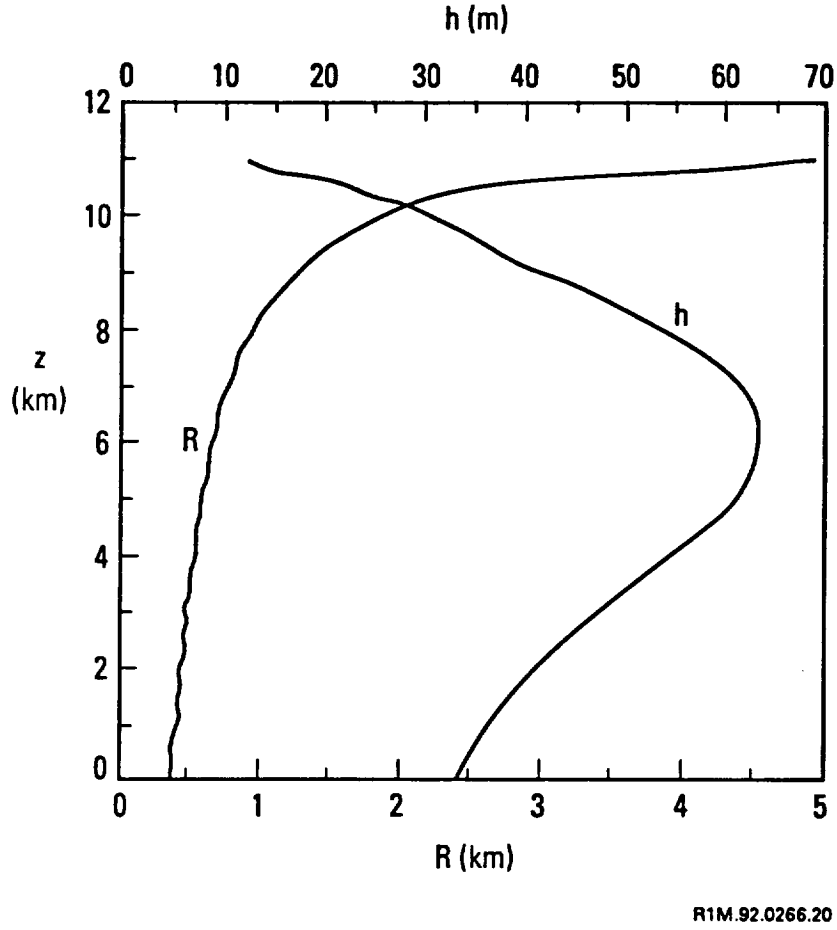

Fig. 4. For the nominal case [defined by the sounding of Fig. 1 and the parameter assignments of Eq. (17)], the radial displacement of the eyewall, R(z), and the thickness of the eyewall, h(z).

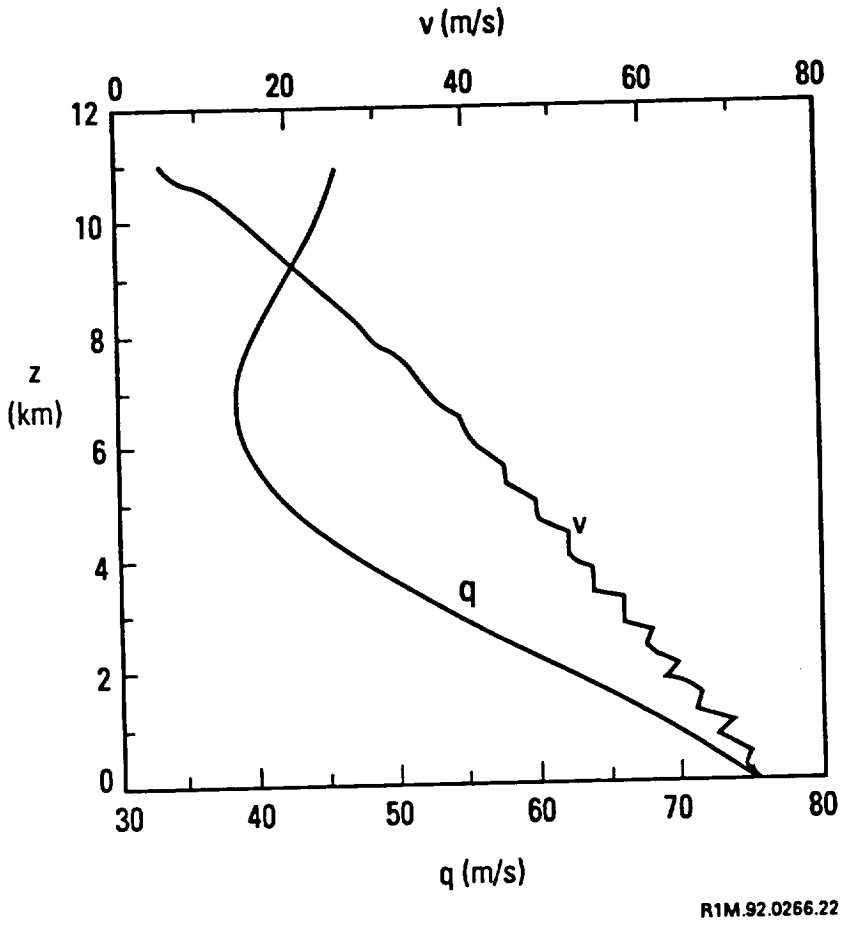

Fig. 5. For the nominal case, the streamwise velocity component in the eyewall, q(z), and the swirl velocity component, v(z).

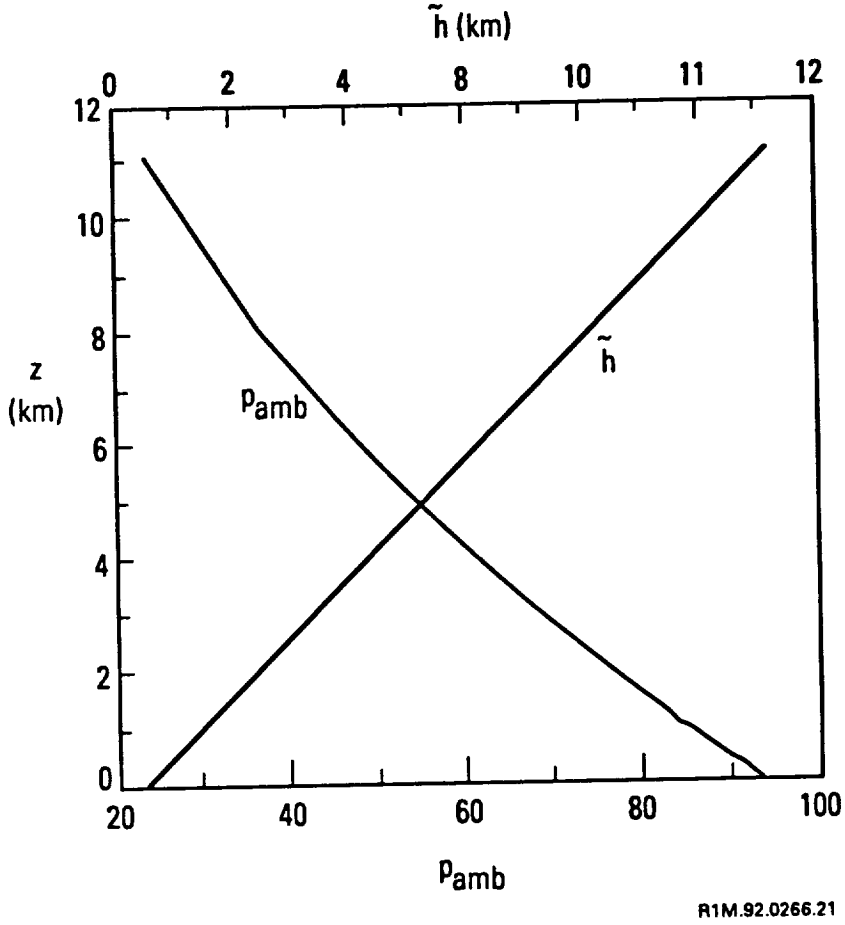

Fig. 6. For the nominal case, the pressure at the potential-vortex/eyewall interface, $p_{amb}(z)$, and the height at the periphery at which the pressure p_{amb} occurs, $\tilde{h}(z)$.

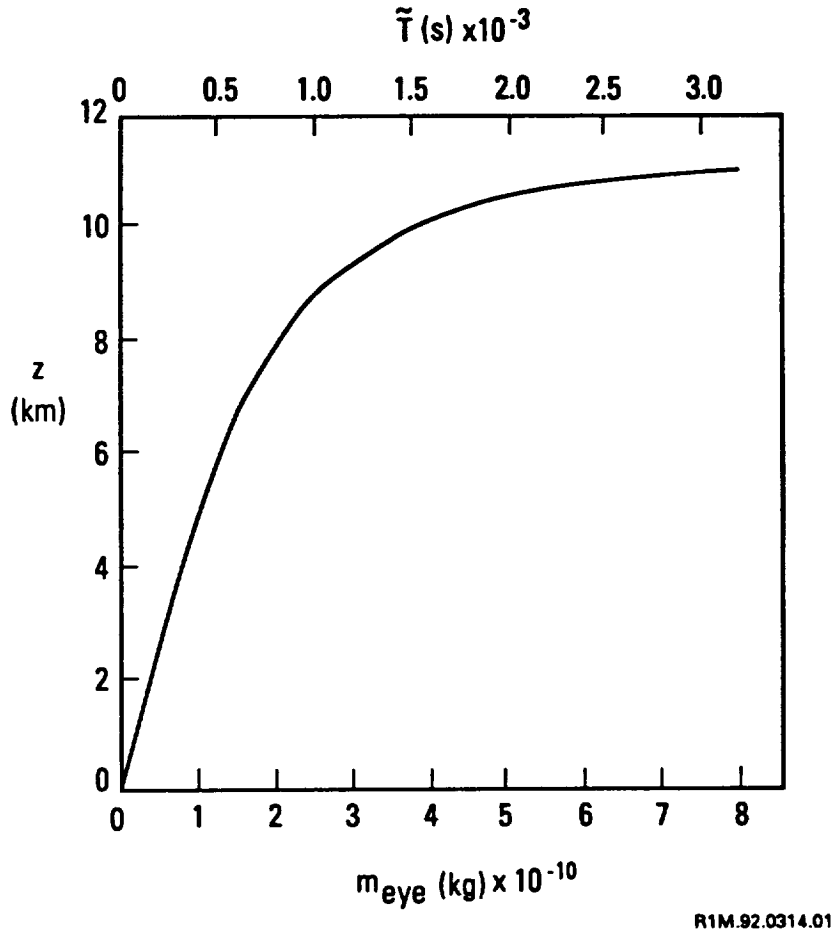

Fig. 7. For the nominal case, the mass in the eye as a function of altitude, $m_{eye}(z)$, and the filling time $\tilde{T}(z)= m_{eye}(z)/\dot{m}_{eyewall}$, where $\dot{m}_{eyewall}$ is defined by Eq. (14).

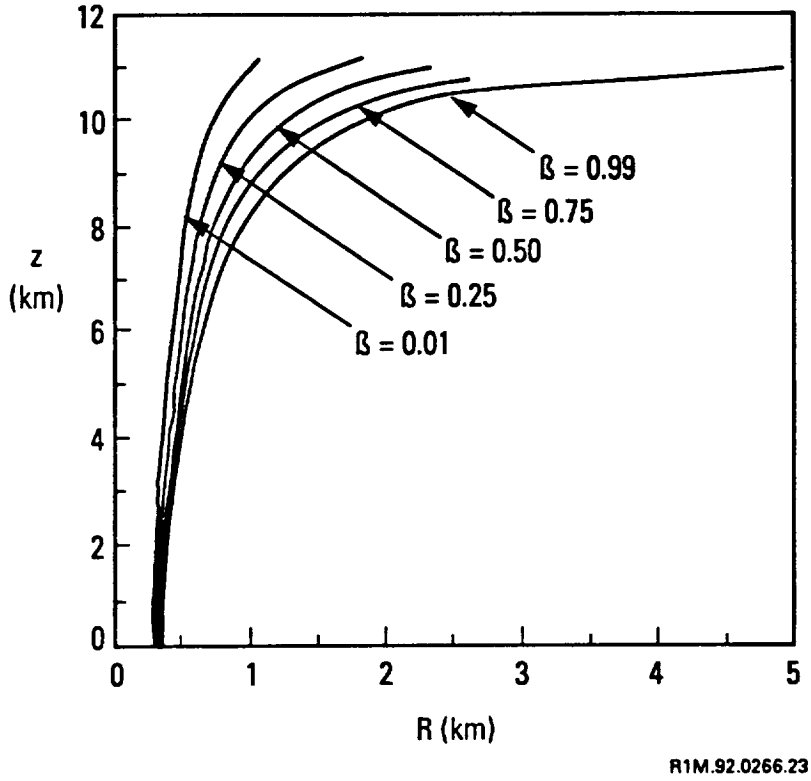

Fig. 8. The radial displacement of the eyewall, R(z), for several values of the parameter β, related to the vertical distribution of the angular momentum at the periphery, where β = 1 is an axially invariant distribution and β = 0 is strongly stratified. All other parameters and functions are held at their nominal values (and β = 0.99 is nominal).

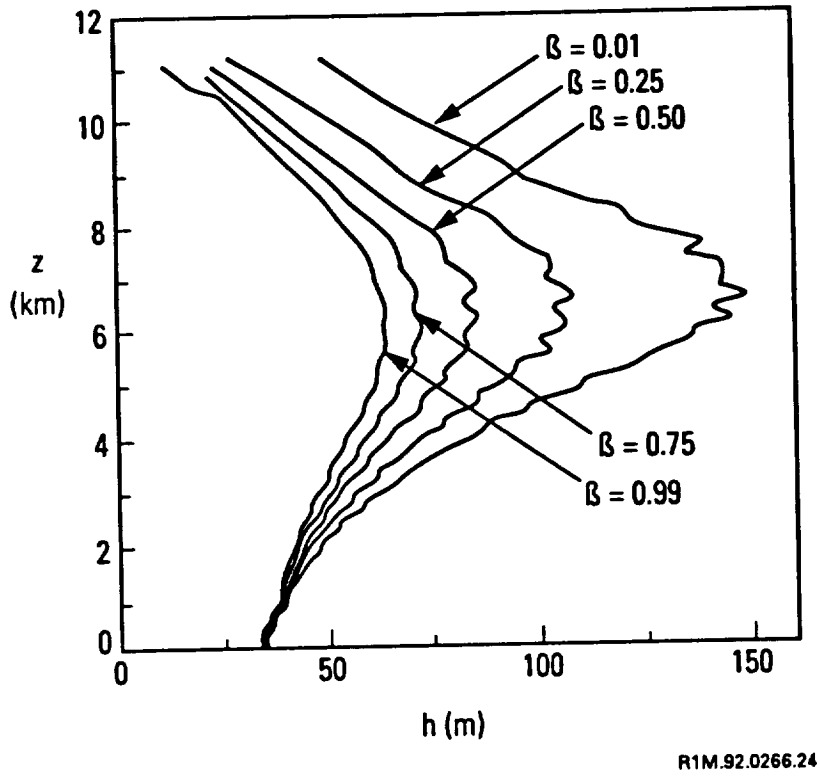

Fig. 9. The eyewall thickness, h(z), to complement the results of Fig. 8.

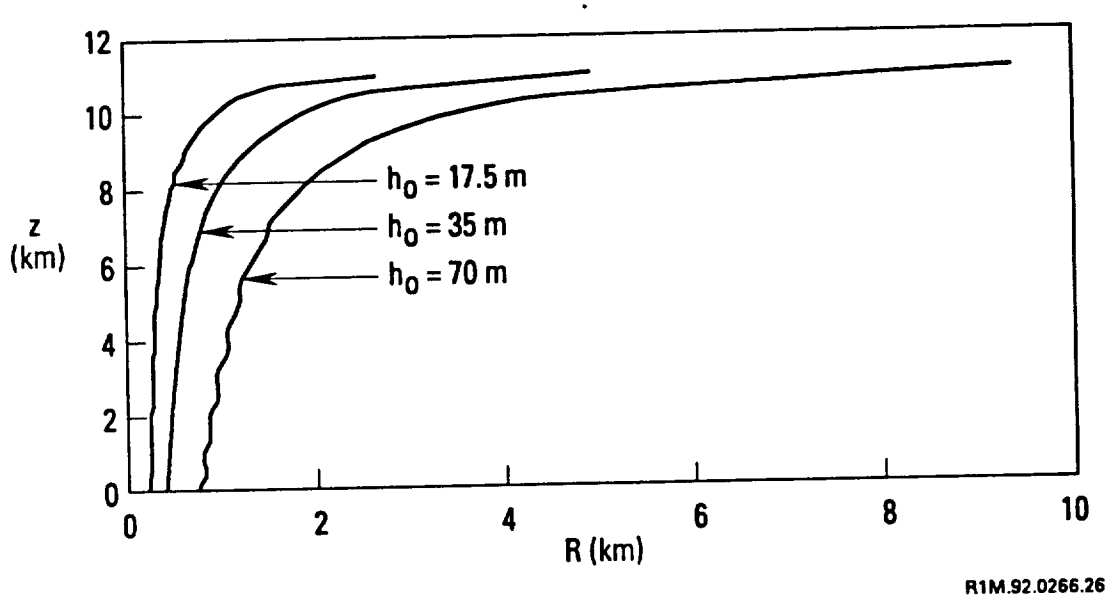

Fig. 10. The radial displacement of the eyewall, R(z), for three values of the initial thickness h_o, all other parameters and functions being held at their nominal values (with h_o = 35 m being nominal). Of course, the initial curvature ε [Eq. (18)] varies with h_o, since the ratio (R_o/h_o) is fixed at its nominal value, 10.

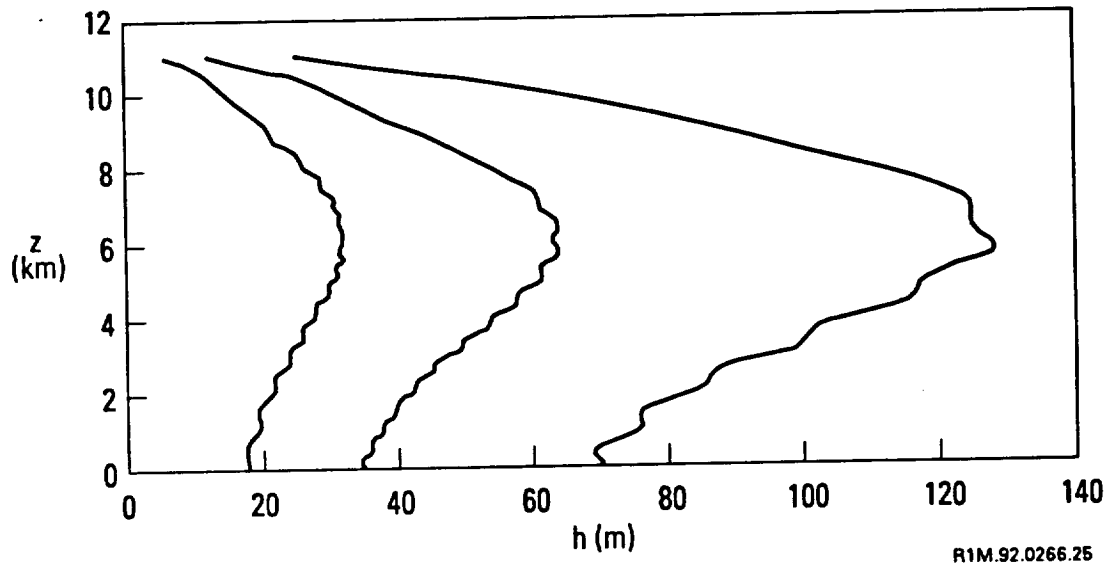

Fig. 11. The eyewall thickness, h(z), to complement the results of Fig. 10.

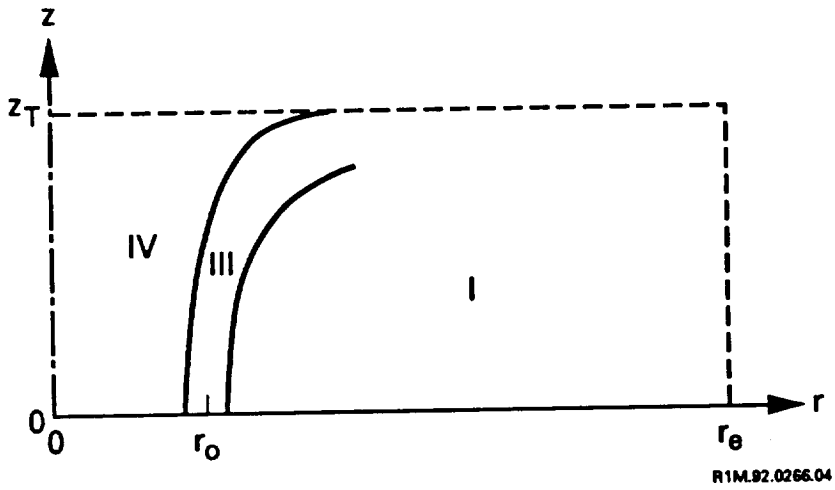

Fig. 12. A simplified schematic of the structure of an axisymmetric two-cell vortex convenient for thermohydrostatic computation. The surface-friction layer II and the turnaround (Fig. 3) have been omitted; in the above sketch, the surface frictional layer does not separate smoothly, and the pressure at the base of the eyewall (region III) appreciably exceeds that at the base of the eye (region IV). For a less intense, one-cell vortex, no eye is present, and $r_o \rightarrow 0$, so region III (no longer termed an eyewall) envelopes the axis of symmetry.

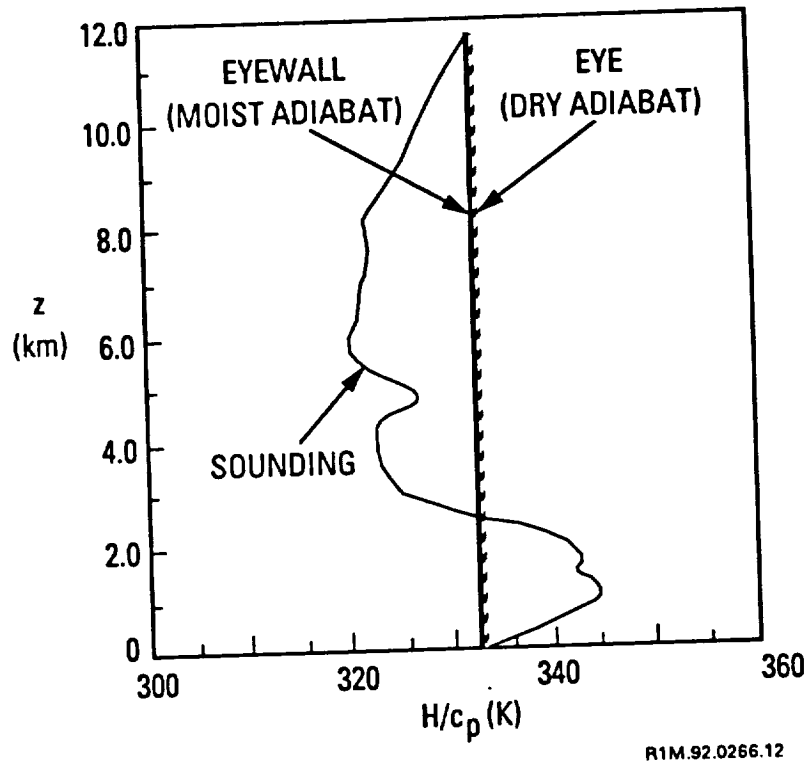

Fig. 13. The total-static-enthalpy profile H(z) associated with three columns of fluid for the model of Fig. 12, with the sounding of Fig. 1 holding at the periphery.

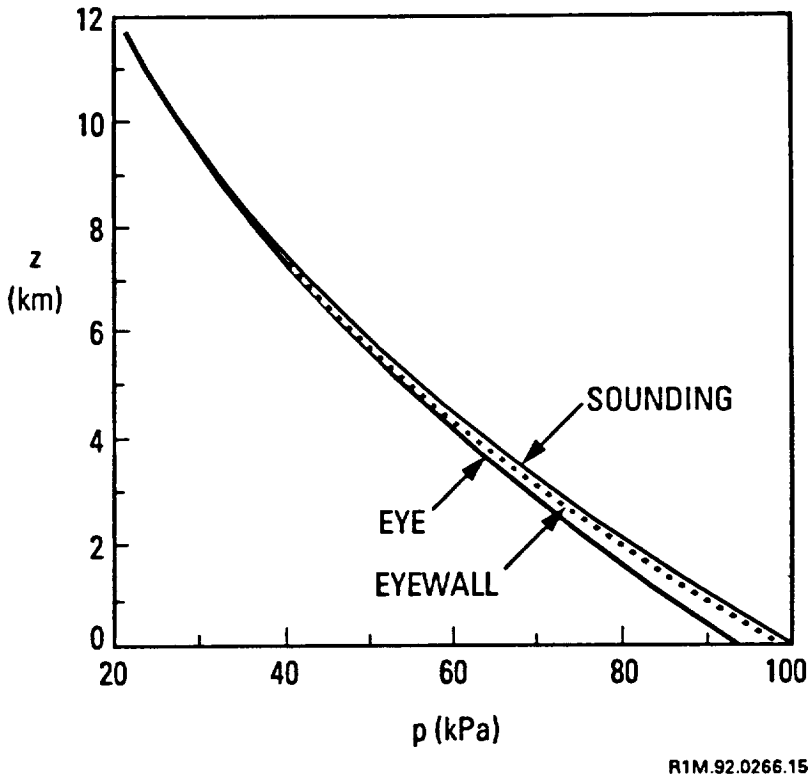

Fig. 14. The pressure profile p(z) associated with three columns of fluid for the model of Fig. 12, with the sounding of Fig. 1 holding at the periphery.

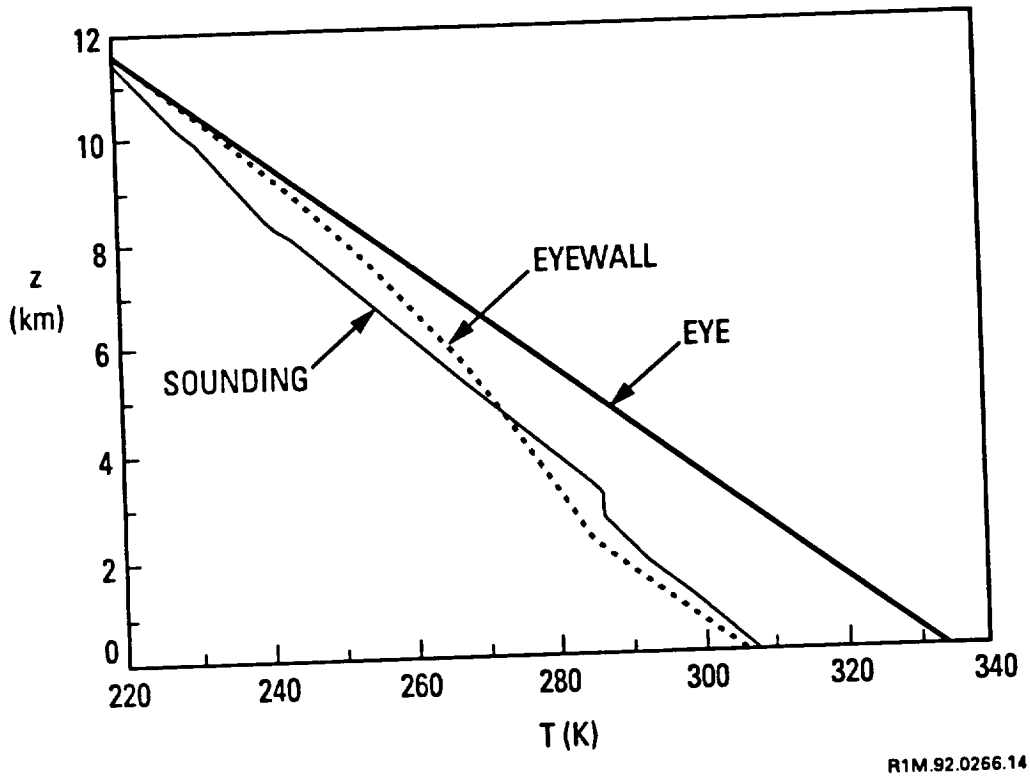

Fig. 15 The temperature profile T(z) associated with three columns of fluid for the model of Fig. 12, with the sounding of Fig. 1 holding at the periphery.

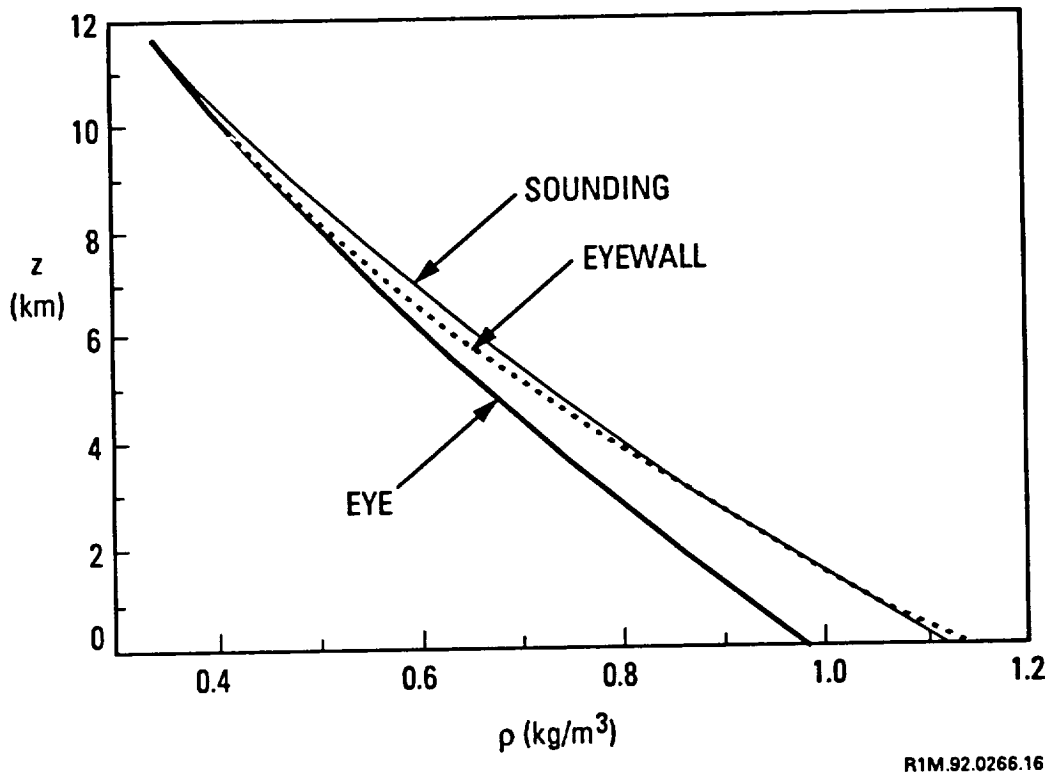

Fig. 16. The density profile $\rho(z)$ associated with three columns of fluid for the model of Fig. 12, with the sounding of Fig. 1 holding at the periphery.

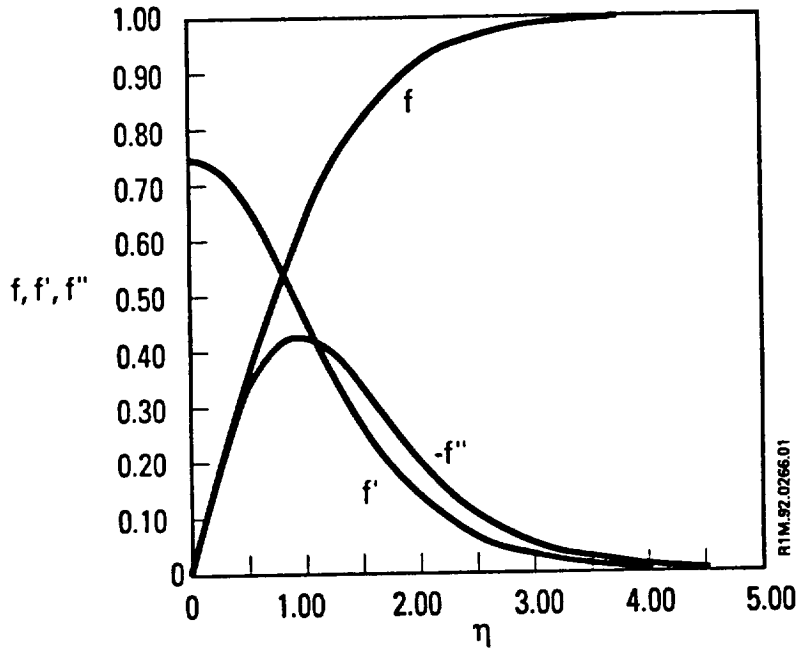

Fig. 17. For spatially constant viscosity, results related to the radial and axial velocity components for the outer, preponderant portion of the boundary layer under the high-speed portion of an impressed vortex. The similarly independent variable η is large for large distances normal to the wall or for small radial distances from the outer edge of the vortex system.

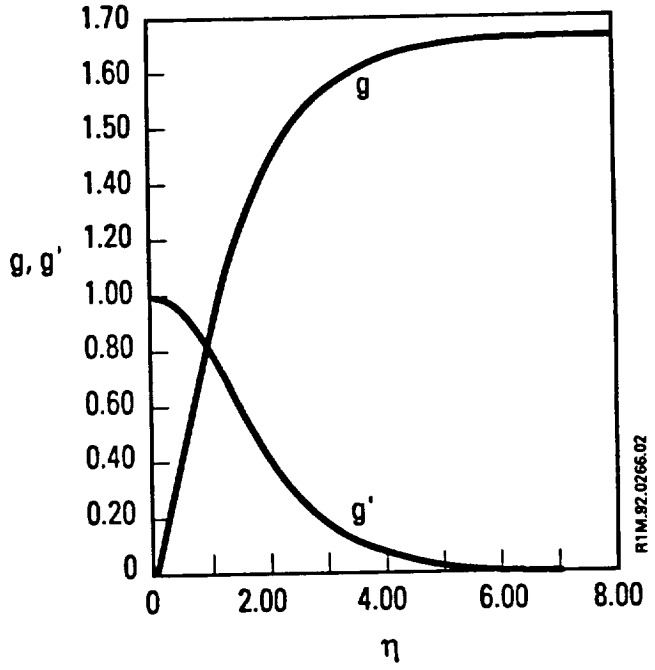

Fig. 18. As a complement to Fig. 17, results related to the swirl-velocity component.

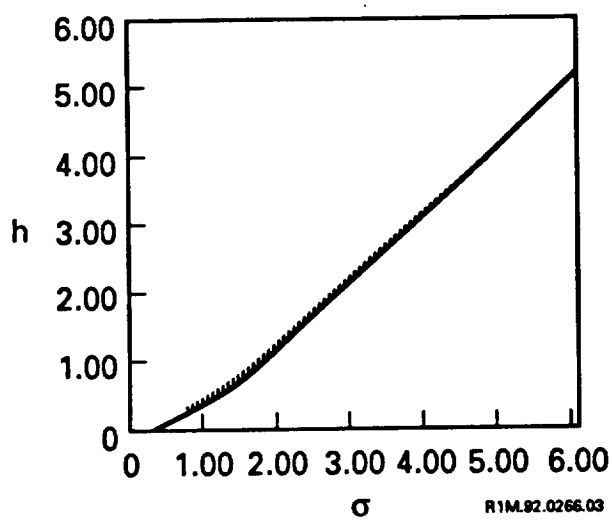

Fig. 19. For spatially constant viscosity, a comparison of numerically computed (dotted curve) and approximate analytic (solid) results for the function $h(\sigma)$, related to the radial inflow in the thin, effectively nonrotating sublayer under the high-speed portion of an impressed swirl. The similarity independent variable σ is large for large distances normal to the wall or for small radial distances from the axis of rotation.

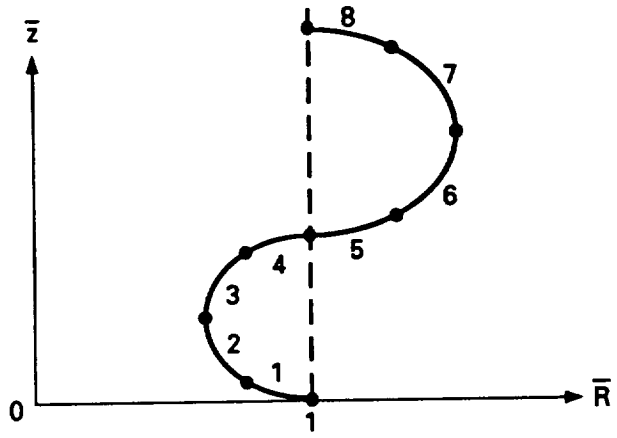

SEGMENT	EQ.	SIGN
1	II	-
2	I	-
3	I	-
4	II	+
5	II	+
6	I	-
7	I	-
8	II	-

R1M.92.0266.06

Fig. 20. For numerical integration of the turnaround, a convenient (but nonessential) eight-segment subdivision is considered, with a segment end-point introduced wherever $\overline{z}_{\overline{R}} = 0$, $\overline{R}_{\overline{z}} = 0$, or $|\overline{R}_{\overline{z}}| = 1$. Equation I is Eq. (D.8); Eq. II is Eq. (D.12), derivable from Eq. (D.8) by an interchange of the roles of the independent and dependent variables. The "sign" column indicates the sign locally adopted for the last turn in Eq. (D.8) or Eq. (D.12), as appropriate.

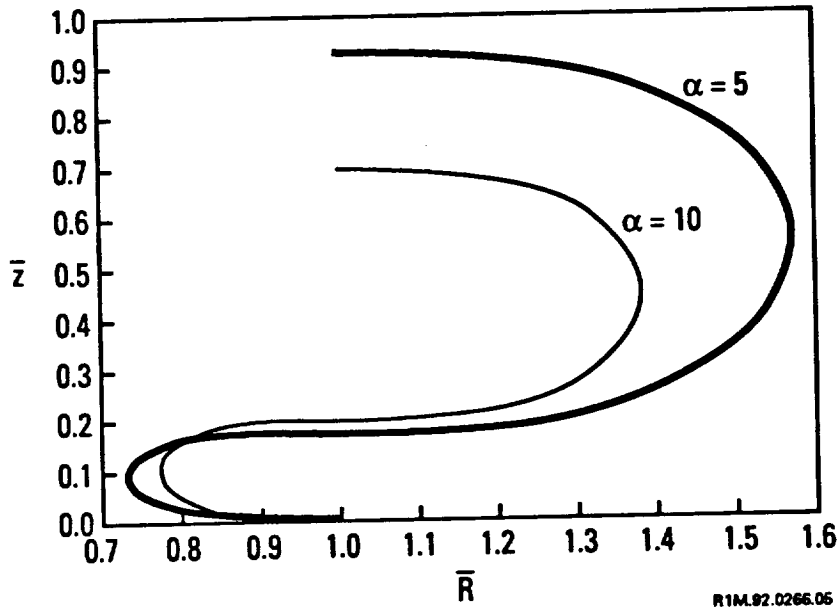

Fig. 21. The dimensionless radial displacement, $\bar{R}(\bar{z})$, of a smoothly separated surface-inflow layer, over one cycle (incursion, then excursion, with increasing attitude $\bar{z}$) of the turnaround. As the geometric ratio α increases, the minimum value of $\bar{R}$ increases, so the local peak swirl exceeds the thermohydrostatically estimated peak value by a smaller amount.